Dual-Band Infrared Scheimpflug Lidar Reveals Insect Activity in a Tropical Cloud Forest

Santos, Victor; Costa-Vera, Cesar; Rivera-Parra, Pamela; Burneo, Santiago; Molina, Juan; Encalada, Diana; Salvador, Jacobo; Brydegaard, Mikkel

Published in:
Applied Spectroscopy

DOI:
10.1177/00037028231169302

2023

Document Version:
Peer reviewed version (aka post-print)

Dual-Band Infrared Scheimpflug Lidar Reveals Insect Activity in a Tropical Cloud Forest

Journal:	*Applied Spectroscopy*
Manuscript ID	ASP-23-0007.R2
Manuscript Type:	Submitted Manuscript
Date Submitted by the Author:	17-Mar-2023
Complete List of Authors:	Santos Logroño, Víctor; Escuela Politecnica Nacional, Dept. Fisica; Costa-Vera, Cesar; Escuela Politecnica Nacional, Dept. Fisica; Escuela Politecnica Nacional Rivera-Parra, Pamela; Escuela Politecnica Nacional, Dept. Biología Burneo, Santiago ; Pontificia Universidad Católica del Ecuador Escuela de Ciencias Biológicas, Museo de Zoologia-QCAZ Molina, Juan; Escuela Politecnica Nacional, Dept. Fisica Encalada, Diana; Universidad Tecnica Particular de Loja, Dpto. de Economía Salvador, Jacobo; Lund University Department of Physics Brydegaard, Mikkel; Lund University, Dept. Physics
Manuscript Keywords:	Scheimpflug entomological Lidar, Optical aerofauna monitoring, Optical insect characterization, Dual-band CW Lidar, Scheimpflug Light Detection and Ranging, Entomological Sensor, Dual-Band Ranger, Insect Activity, Foggy Conditions, Frequency Domain
Abstract:	We describe an entomological dual-band 808 and 980 nm lidar system which has been implemented in a tropical cloud forest (Ecuador). The system was successfully tested at a sample rate of 5 kHz in a cloud forest during challenging foggy conditions (extinction coefficients up to 20 km-1). At times, the backscattered signal could be retrieved from a distance of 2929 m. We present insect and bat observations up to 200 m during a single night with an emphasis on fog aspects, potentials, and benefits of such dual-band systems. We demonstrate that the modulation contrast between insects and fog is high in the frequency domain compared to intensity in the time domain, thus allowing for better identification and quantification in misty forests. Oscillatory lidar extinction effects are shown in this work for the first time, caused by the combination of dense fog and large moths partially obstructing the beam. We demonstrate here an interesting case of a moth where left- and right-wing movements induced oscillations in both intensity and pixel spread. In addition, we were able to identify the dorsal and ventral sides of the wings by estimating the corresponding melanization with the dual-band lidar. We demonstrate that the wing beat trajectories in the dual-band parameter space are complementary rather than covarying or redundant, thus dual-band entomological lidar approach to biodiversity studies is feasible in situ and endows species specificity differentiation. Future improvements are discussed. The introduction of these methodologies opens the door to a wealth of possible experiments to monitor, understand and safeguard the biological resources of one of the most biodiverse countries on earth.

Dual-band Infrared Scheimpflug lidar reveals insect activity in a tropical cloud forest

VICTOR SANTOS[1], CESAR COSTA-VERA[1*], PAMELA RIVERA-PARRA[2], SANTIAGO BURNEO[3], JUAN MOLINA[1], DIANA ENCALADA[4], JACOBO SALVADOR[5], AND MIKKEL BRYDEGAARD[5,6]

[1]*Dpto. de Física, Escuela Politécnica Nacional, Av. Ladrón de Guevara E11-253, Quito 170525, Ecuador*
[2]*Dpto. de Biología, Escuela Politécnica Nacional, Av. Ladrón de Guevara E11-253, Quito 170525, Ecuador*
[3]*Pontificia Universidad Católica del Ecuador, Avenida 12 de Octubre 1076, Quito*
[4]*Dpto. de Economía, Universidad Técnica Particular de Loja, San Cayetano Alto, Loja, Ecuador*
[5]*Dept. of Physics, Lund University, Sölvegatan 14c, 22362 Lund, Sweden*
[6]*Norsk Elektro Optikk AS, Østensjøveien 34, 0667 Oslo, Norway*
**cesar.costa@epn.edu.ec*

Abstract:

We describe an entomological dual-band 808 and 980 nm lidar system which has been implemented in a tropical cloud forest (Ecuador). The system was successfully tested at a sample rate of 5 kHz in a cloud forest during challenging foggy conditions (extinction coefficients of 20 km^{-1}) for the first time. At times, the backscattered signal could be retrieved from a distance of up to 2929 m. We present insect and bat observations up to 200 m during a single night with an emphasis on fog aspects, potentials, and benefits of such dual-band systems. We demonstrate that the modulation contrast between insects and fog is high in the frequency domain compared to intensity in the time domain, thus allowing for better identification and quantification in misty forests. Oscillatory lidar extinction effects are shown in this work for the first time, caused by the combination of dense fog and large moths partially obstructing the beam. We demonstrate here an interesting case of a moth where left- and right-wing movements induced oscillations in both intensity and pixel spread. In addition, we were able to identify the dorsal and ventral sides of the wings by estimating the corresponding melanization with the dual-band lidar. We demonstrate that the wing beat trajectories in the dual-band parameter space are complementary rather than covarying or redundant, thus dual-band entomological is feasible *in situ* and benefits species specificity. Future improvements are discussed. The introduction of these methodologies opens the door to a wealth of possible explorations to monitor, understand and safeguard biological resources in the most biodiverse countries on earth.

1. Introduction

Assessment of biodiversity is fundamental for understanding complex interactions[1] and for preserving ecosystems. Factors such as rainfall, mountainous topography, and vicinity to the equator all increase species richness[2,3] of trees, birds, mammals, reptiles, amphibians, and insects. Unfortunately, many important biodiversity hotspots, such as Andean tropical rainforests, remain poorly studied[4]. Species inventorying in a tall standing rainforest is challenging; vegetation and dense fog limit visibility and insect species are vertically stratified[5]. Conventional surveys include traps and sweepnets[6], but generally, traps and baits are biased[7] and limit studies to subgroups of species. As an example, hundred species of fruit-feeding butterflies can be found at a single Ecuadorian site[8]. More general estimations of insect species in the richness in tropical virgin forests are costly and complicated[9,10]. Analysis of caught

samples may also be exceedingly laborious, metabarcoding can detect the presence of species in genetic databases[11-13] but fail to report on abundances. Innovative solutions with machine vision and robotics may be required to automate catch analysis[14].

Photonic monitoring approaches[15-18] may be able to estimate the insect species richness in real-time *in situ*, without biasing, sample handling, or great collecting efforts. Furthermore, entomological lidar could access diversity throughout tall canopies of virgin forests, which are known to foster higher diversity.

The aim of this paper is to present a novel dual-band (808 and 980 nm) entomological lidar in Ecuador. In particular, we showcase the feasibility of remotely observing insects *in situ* during severely foggy conditions (20 km^{-1}) for the first time and demonstrate how two bands provide complementary information and can be expected to distinguish more species.

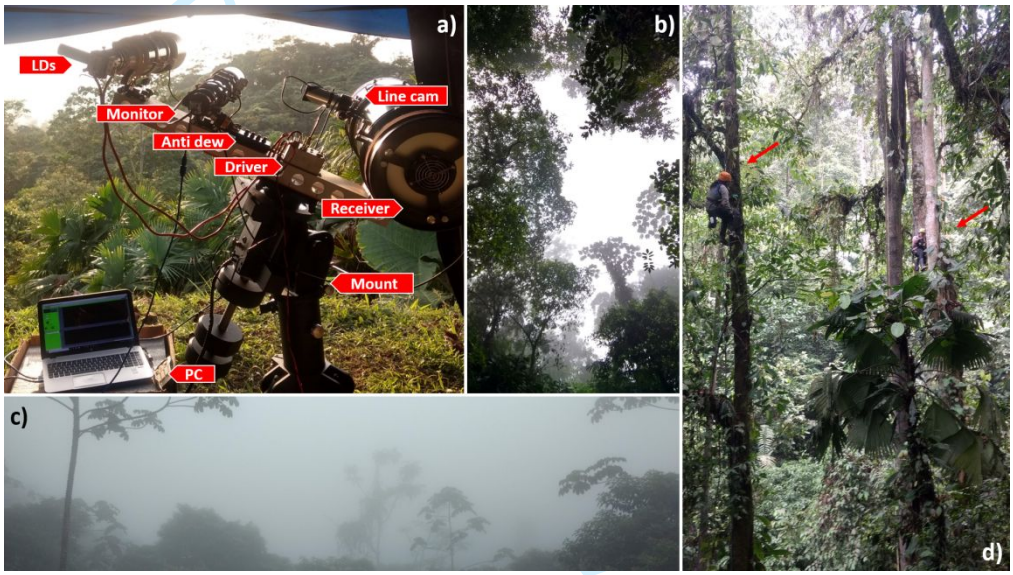

Fig. 1. **a)** Entomological-lidar system and its main components overlooking the *Jardin de los sueños* private forest, during a clear moment (17:30). **b)** Photo displaying the top of canopies at ~30 m over ground disappearing into the mist (9:30), **c)** A view from lidar toward valley at noon (12:05), typical of the field campaign days. The mist is impenetrable. **d)** Ecological studies in tropical virgin forests are challenging due to topography, tall vegetation structure, and stratification of ecological niches, here two chiroptologists install a bat net 20 m above ground.

2. Methods

2.1 Field site

The study was carried out in the private reserve "Bosque Protector Jardín de los Sueños", an evergreen forest (~500 m asl) at the foot of the western Andean ridge in Cotopaxi province, Ecuador. The annual mean temperatures are 18-24 °C with a mean relative humidity of 86%. There is an average rainfall of 7 m/year, and the dry season extends between July and December, while the rainy season goes from January to May. This mountainous forest is part of the remaining Chocó rainforest region which covers most of Colombia's Pacific coast. The location presents fog and mist through most of the day all year around. The forest includes primary virgin vegetation with tree canopies above 50 m (Fig.2d) and some secondary forest at the edges. The site is a biodiversity hotspot and hosts a broad range of animal species on the ground, throughout the canopy, and free-flying. Because of this and other factors, this reserve has been identified as an important wildlife refuge for all taxonomic groups, with a special emphasis on bats. In the year 2021, the reserve was designated as an important preservation spot by the Ecuadorian Bat Conservation Program. This location provides an interesting place

to study bat-prey interactions. Forest patches such as this act as a biodiversity source for the surrounding territories and is a crucial fountain of ecosystem services such as pollination, seed dispersal, and refuge for pest predators.

2.2 Test range

For the feasibility test, the lidar system was transported to the field site and mounted in an open-side garage tent (Fig.1a, 0°50'15.30"S, 79°12'18.64"W). The system was powered with a 2 kW generator placed at about 25 m in distance. The lidar was overlooking a descending skirt toward a valley covered by forest. This work reports results obtained from a transect terminating in a coffee plantation (Fig.2d. 0°50'54.92"S, 79°13'44.17"W), some 2950 m from the lidar. In its path, the beam descended at 4.5° from 577 m to 346 m asl (Fig.2c). Around 800 m, the beam was surrounded by tall canopies on both sides (Fig.2e).

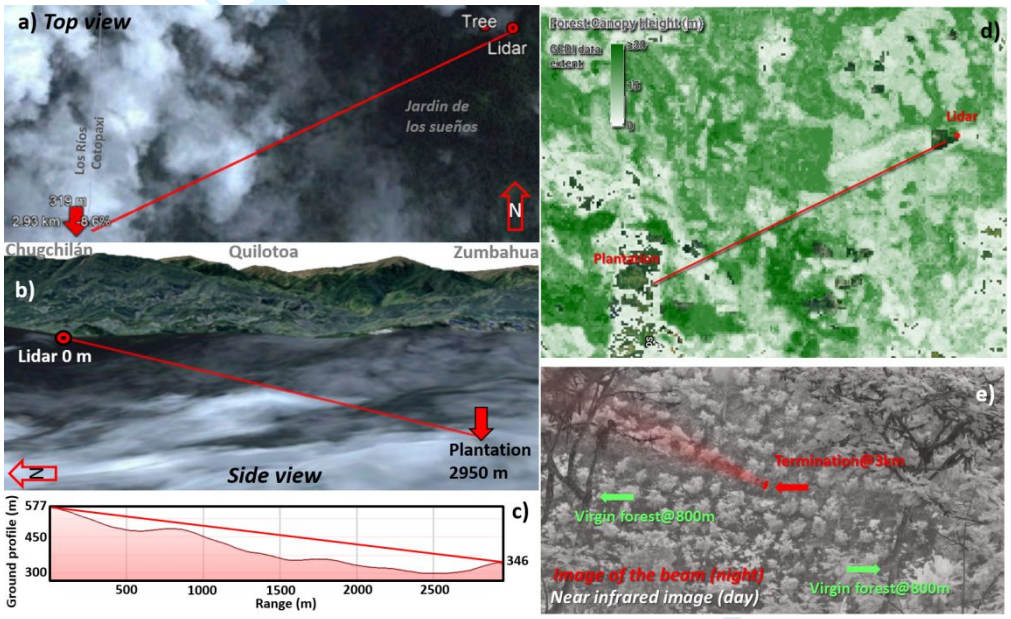

Fig. 2. Lidar transect: **a)** Top view from an overcast satellite image of the cloud forest. The laser beam terminates in the valley after propagating almost 3 km. **b)** The field site is on the intermediate lowlands, and is part of the great pacific rainforest *El Chocó*, descending from the Andes to the Pacific Coast. **c)** The beam was sent 4.5° inclined through the valley, at times with vegetation on both sides. **d)** Average vegetation height from space-borne lidar, the darker green areas indicate primary forest. **e)** Despite limited visibility by eye, an infrared near-infrared (0.8-1 µm) camera can at times form an image of the coffee plantation 3 km away where the beam terminates. The tall vegetation at closer range is seen on both sides of the beam. A nighttime image is superimposed in red to display the backscattering in the air and the beam remote termination spot.

2.3 Dual-band entomological lidar

The developed entomological lidar was designed according to the Scheimpflug lidar principle[19-22]. This method employs multiplexed continuous wave lasers and triangulation in combination with the Scheimpflug focus strategy whereby sharp focus can be accomplished at all distances simultaneously despite the use of large apertures. This, in turn, allows for fast acquisition up to several kHz and capturing of the oscillatory properties of non-stationary insect targets[16,23]. Our system resembles previous systems on other continents[16,24-26], and it also consists of a transmitter and a receiver mounted on an aluminum baseline frame with an 845 mm separation (see Fig.1a and Fig.3). This baseline is in turn, mounted on a heavy-duty motorized tripod (EQ8, SkyWatcher, China) for stable positioning and pointing. The transmitter is comprised of a beam

expander with Ø120mm/f600mm, (Startravel 120OTA, SkyWatcher, China) with an upgraded focal stage (Monorail R96, Teleskop Service, Germany). A dichroic beam splitter (Fig.3a) is installed on a rotary stage at the focal port of the beam expander (#69-907, Edmund Optics, USA with B4CRP/M, Thorlabs, USA). Two c-mount diode lasers are installed on the branches of the beam splitter: a 5W, 808 nm diode, and a 3W, 980 nm diode (MLD-808-5000 and MLD-980-3000, CNI laser, China). Both beams are TM polarized with an aperture of 100 µm and rod lenses for matching the divergences. TM polarization implies that the E-field is parallel to the baseline of the lidar. The diodes are ordered with a Fast Axis Collimating lens precision glued to the device. Hereby divergence is 8° in both axes, and the collection efficiency by the F/5 telescope becomes 82%. The laser beam splitter mounting stage allows for a precise super-positioning of the two sources, while a cage system mounting permits the relative focus adjustment of the two diodes to compensate for the achromatic focal shift of the expander. For lidar overlap purposes, the beam expander is mounted on the baseline with a tangential mount (Stronghold, Baader, Germany).

The receiver is a Ø250mm/f1000mm Newtonian reflecting telescope (Quattro-10S, SkyWatcher, China). A custom wedge is installed in the focal port. This wedge holds a ø50mm RG780 long pass filter (Edmund Optics, USA). Further, the wedge supports a linear CMOS camera (OctoPlus EV71YO1CUB2210-BB1, Teledyne e2v Imaging, USA). This 12-bit USB3 camera has 2048 pixels of 10×200µm each and can reach line rates of 80 kHz. The camera emits a kHz strobe pulse at every exposure, this signal is used to alternate the laser driver between 3 states: dark, 808 nm and 980 nm (see Fig.3b). This lock-in multiplexing method is also described in previous work[27-29]. Light interaction with insects in the NIR region is dominated by melanization and thinfilm[30] effects. Fig.3c displays the band placement in relation to typical melanization of insects[31]. Fig.3d displays the ability of the two bands to produce resonant backscatter depending on the wing thickness for typical insect wing thicknesses[32,33].

Finally, the lidar is equipped with an additional refracting telescope Ø102mm/f500mm (StarTravel, SkyWatcher, China) with a NIR sensitive USB3 camera (acA1920-155um, Bassler, Germany) for surveillance and beam alignment purpose (see Fig.2e). All telescopes are fitted with anti-dew bands to prevent water condensation on the optics (Astroshop, Germany). A complete components list is available from the corresponding author upon request.

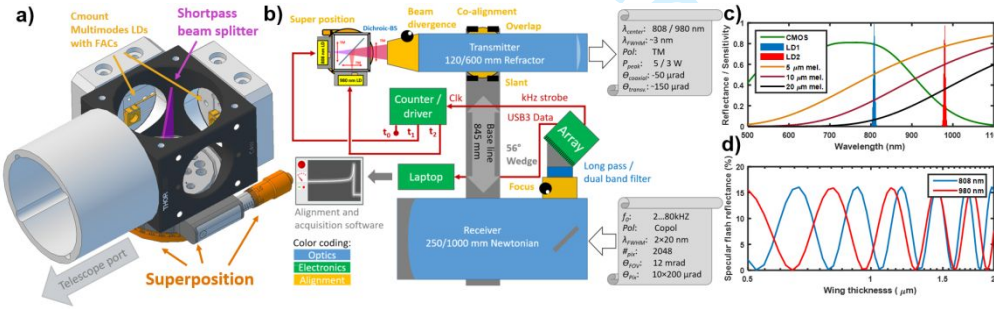

Fig. 3. Technical details of the dual-band lidar system. **A)** Close-up of dual-band laser diode assembly. The emission cones of two multimode laser diodes with fast-axis-collimators (FACs) are combined by a dichroic shortpass beamsplitter on a precision alignment stage. **b)** Schematics of the Scheimpflug lidar system. The sensor strobe signal alternates the laser driver between dark, 808 nm and 980 nm. **c)** Spectral overview displaying the CMOS array sensitivity and the emission of the two lasers. The reflectance model for insect targets with three different equivalent pathlength of pure melanin is displayed for reference. **d)** Thin film model of the resonant backscatter for the two lidar bands as a function of typical insect wing thicknesses.

2.4 System operation and data collection

The system is operated from an adjacent laptop. The computer produces a preview of the infrared monitor camera for beam alignment purposes. The actual lidar data acquisition is done by a custom-made, real-time, user interface programmed in LabView (National Instruments, USA). The program was set to capture frames of 30000 exposures × 2048 pixels, it then demultiplexes the frame into a 3D tensor of 10000 exposures × 2048-pixel × 3 time slots (dark/808nm/980nm). The dark timeslot is identified by its minimum average total intensity and is subtracted from the 808 and 980 nm timeslot. The program then displays the minimum/median / maximum pixel profile (range echo) for each band. Also, the dark signal is displayed in a separate graph. The graphs update every time a new frame is acquired and 12bit raw intensity data is continuously saved at an external USB3 drive. Each filename is time stamped and each frame file is 120 Mb. In this work the line rate was set to 5 kHz, line period 200 µs, exposure time 180 µs, pre-amplifier 4x, gain 8x, and bias 0 counts.

3. Results

Our report from this initial work focuses on the detection of insects under a dense fog, which is particularly relevant for monitoring the biodiversity of cloud forests under real natural conditions. In Fig.4a, the first light of the Ecuadorian lidar is presented in a time-range map displaying the first half hour of the measurements. The color coding includes the max signal from both bands as well as the median from the 808 nm band. Insects show up as green dots, bats are seen as yellow dots while the fog is identifiable in shades of blue and white. Artifacts from fireflies are also seen on some occasions. Initially, back-scattered light is retrieved over the full range of 3 km, the fog then closes in and extinguishes light after 100 m. The plot is made from 250 lidar files, each spanning 6 s. In Fig.4b we display the time and range resolved frequency content in a single file. Even though the fog is much stronger in backscatter compared to insects, the frequency content of fog is relatively low. This implies that it may be challenging to contrast out insects inside fog in the intensity-time domain while the contrast in the power-frequency domain is much higher.

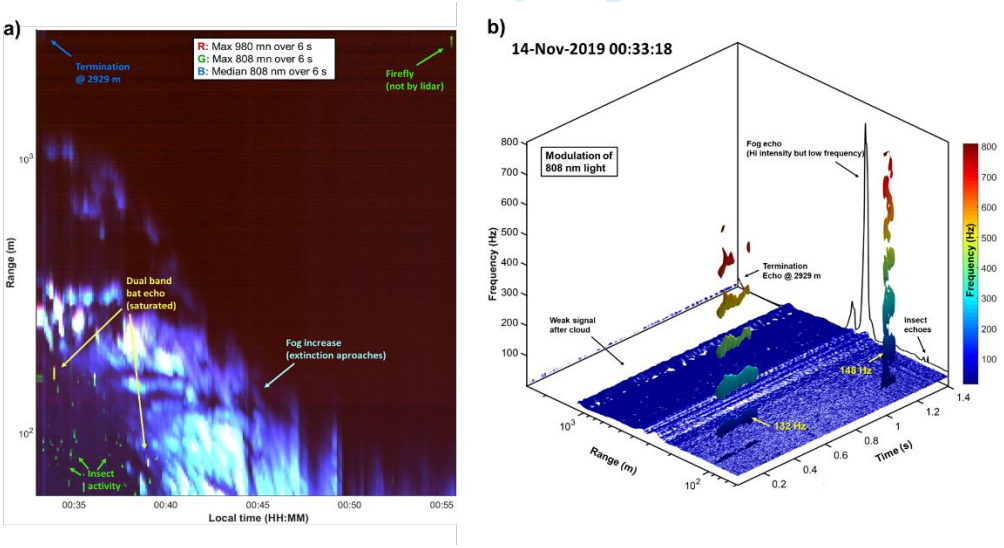

Fig. 4. Lidar data: **a)** The first half hour of the reported pilot field test is displayed in a time-range lidar map. Each column in the map represents a 6 s datafile. The maxima values of 980 nm backscatter are displayed as red, maxima of 808 nm are displayed as green and, median values of 808 nm, which is insensitive to insects, are displayed as blue. The beginning represents a rare occasion with a signal visible all the way to the termination 3 km away, the visibility then decreases, and light is extinguished within the first 100 m. Insects show up as green dots on the map and bats display strong echoes in both bands. Fireflies were also observed both visually and by the instrument. These signals are unrelated to the modulation of the lasers and their actual distance cannot be deduced. **b)** Range resolved spectrogram

of the lidar data illustrated by a 3D isosurface. The signal from the air and fog contributes low frequencies and is displayed in blue at the bottom of the plot. Two insects with distinct wing beat frequencies intercept the beam at a 100 m distance. The mean echo is displayed in the back panel in linear scale, the signal is dominated by an intense peak from a cloud layer at a 300 m distance, and smaller echoes from the two insects and the termination are also seen. Note that the contrast between fog and insects is poor in the echo intensity domain but great in the frequency domain.

In Fig.5 we highlight the first insect observation at 90 m of distance during 200 ms (same file as Fig.4b). The signal from the insect is small compared to the fog layer at 300 m distance, still the fog is thin enough at this point that allows light to reach the termination at 3 km and return. Fig.5b also shows that the 980 nm signal is one order of magnitude weaker than the 808 nm band. There are multiple reasons for this: 1) weaker laser power, 2) worse spectral response of the detector, and 3) less atmospheric scattering. The echo of the insect is, however, stronger for the 980 nm band, relative to the atmospheric signal. This is because melanin absorbs less in the 980 nm band (See Fig.3c). If the system was white calibrated against a target with flat spectral reflectance, the band ratio from the body signal would be converted into the equivalent absorption path length of pure melanin in microns[31]. For the wing signal this is slightly more complicated since clear wings produce thin film fringes[32,33] (see Fig.3d). Also, the body- and wing signals can be seen in the time domain, as shown in Fig.5c, as a bias envelope and an oscillatory part, respectively. A close inspection of the signal also demonstrates a highly periodic waveform with various features. The frequency content of the signals in Fig.5d indicates a wing beat frequency of 136 Hz. The 100-200 Hz range is a common wingbeat frequency among insects[16,23,32,34], such as flies and beetles, thus we could not make more informed guesses about the family it belongs to, except that we are dealing with a clear-winged insect (not a moth) because of the spiky waveform and the numerous harmonics. This case also demonstrates that the second harmonic is often stronger than the fundamental tone which can be a challenge for a prospective automatic pitch detection[23].

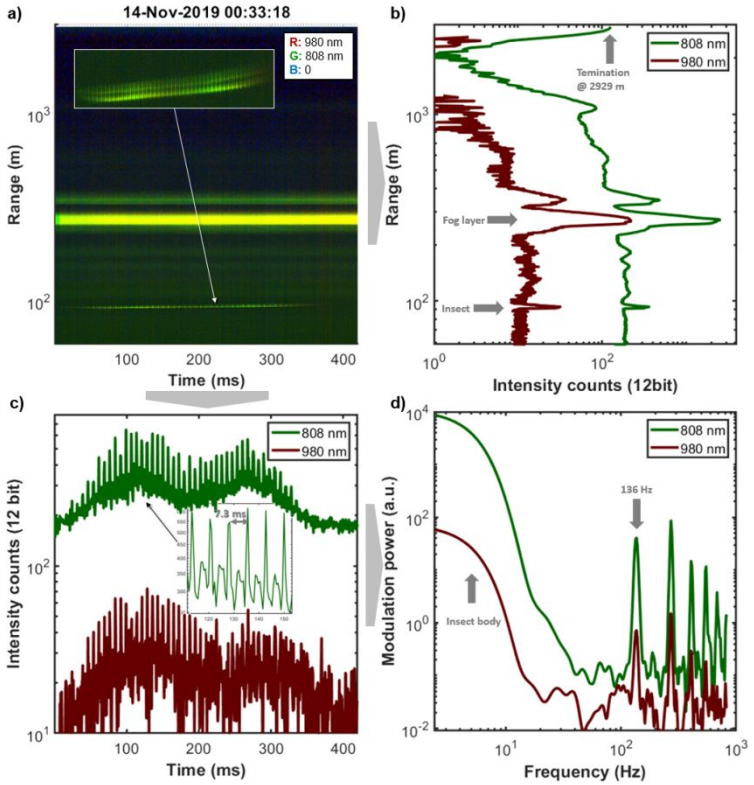

Fig. 5. Example of insect observation by the dual-band lidar: **a)** Dual-band range-time displaying fast oscillatory insect observation *vs.* the slowly changing fog layer. **b)** Average echo of the same data; insect, fog, and termination features are seen at 90, 300, and 2929 m distance respectively. The 980 nm signal is generally one magnitude weaker, but the insect echo is relatively stronger for 980 nm due to the lower atmospheric scattering coefficient and lower absorption by melanin. **c)** Time series of the two bands composed of an oscillatory part from the wings and a bias envelope from the body, the insert displays the reproducibility of the waveform. **d)** In the corresponding power spectrum, the fundamental tone is not necessarily the strongest, but in this case, the second overtone is.

The case highlighted in Fig.6 is instead a moth. This is supported by the hour of flight, the rather low wingbeat frequency, the smooth waveform (low-intensity skewness), and the large apparent size[24,35,36] of 84 mm. Detailed inspection of the signal in Fig.6a reveals a particular dynamics not only in intensity but also in the pixel spread value, the pattern can be explained by scattering contributions from both the dorsal and ventral sides of the left and right wings of the insect. Fig.6a also reveals for the first time oscillatory lidar extinction, where the fog backscatter beyond the moth is shaded when the wings display maximal cross-section. In Fig.6b, the range echoes for each of the two bands are displayed at the times t_{fog} and t_{moth} indicated in Fig.6a. Signal reduction beyond the moth is seen. In theory, lidars can acquire both backscatter and extinction cross sections, and in the applications for entomological lidars is possible to determine both the geometrical cross section and the reflectance at specific bands independently. At this time of the night, laser light was extinguished after 200 m, for guidance exponential decays (round-trip) are superimposed on the graphs in Fig.6b. In this case the moth is detected during extremely dense fog conditions with an attenuation coefficient, μ_{att}, in the order of 20 km^{-1}.

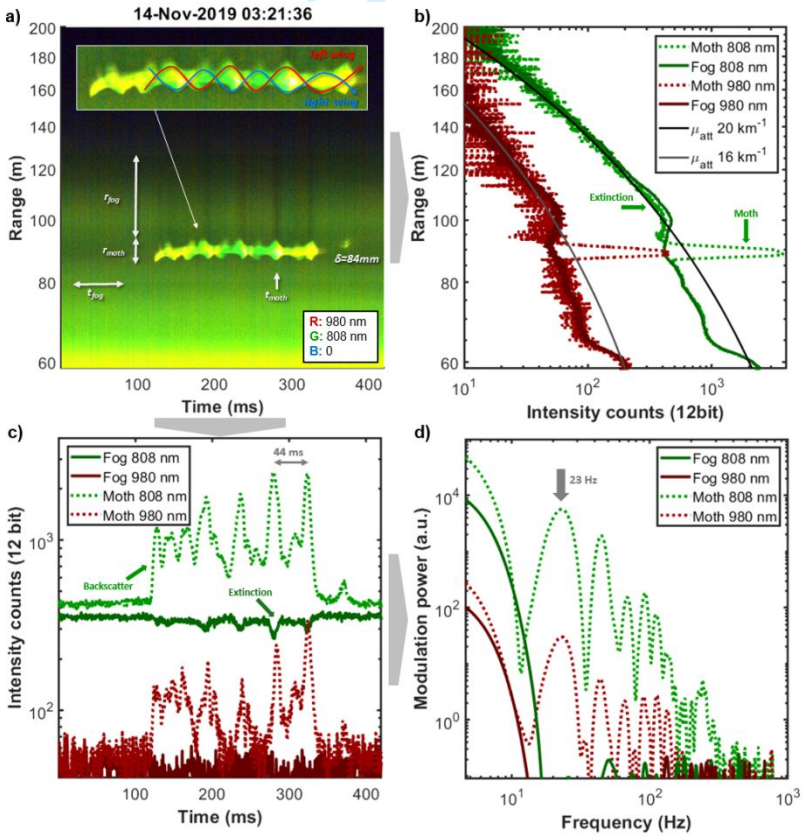

Fig. 6. Lidar observation of a low frequent moth **a)** Dual-band time-range map; dense fog is seen as a gradient across the map. The apparent size was estimated to be 84 mm. The oscillatory extinction of the moth reduces the following backscatter from the fog and periodic shades are seen, e.g., at t_{moth}, when the wing has a maximal cross-section. **b)** Comparison of echoes from fog, t_{fog}, and from fog extinguished by the moth, t_{moth}. A small effect of the extinction is seen. The signal reaches noise levels after 200 m, for visual guidance two exponential decays are inserted with extreme atmospheric attenuation coefficients, μ_{att}, of 16 and 20 km^{-1}.

The benefits of dual-band[37,38] and hyperspectral[39] detection of insects have previously been demonstrated in laboratory settings. In Fig.7 we investigate if the two spectral bands contribute complementary information or if they are only redundant. As evident, the signals in the 808 and 980 nm bands are far from co-varying throughout the ~4 wingbeats seen in Fig.6. The trajectory in the spectral parameter plane in Fig.7 is color-coded by the time during transit. Several repeated features can be observed; straight and fast down strokes, wavy slow upstrokes, a secondary minor peak from the right wing, and a counterclockwise pattern due to contributions from both the melanized dorsal side and the brighter ventral side[31]. The dual-band information retrieved is indeed rich much beyond the simple modulation power spectra in Fig.6, and thus the potential of applying this complementarity to differentiate numerous species is promising. To date, there are well-established methods for signal diversity assessment, deriving from scientific communities of music analysis, speech recognition, and bioacoustics[40,41]. Unfortunately, most audio approaches are insensitive to waveforms and relative phases of harmonics. The concept of including multiple bands and polarizations waveforms in diversity computations is even more exotic in this literature.

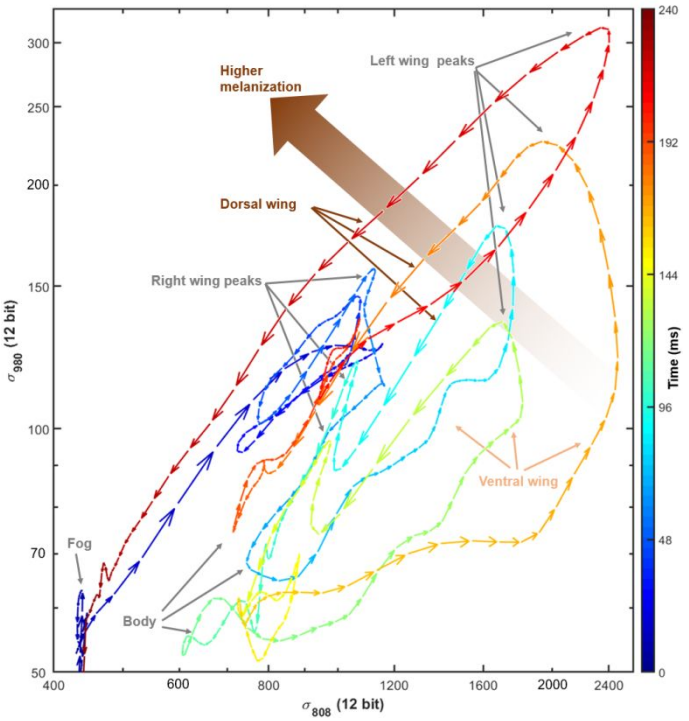

Fig. 7. Dynamics of the backscattering signal from the moth in the two wavelength bands. The color of the arrows indicates time from 0 to 240 ms and the length indicates speed. The signals are not simply co-varying. Despite this slightly challenging graph, repeated features can be observed from the consecutive wingbeats. During each cycle, both left and right wings produce a peak. The downstrokes appear straight and fast whereas the upstrokes appear wavy and slower. Melanization is higher on the dorsal side of the wings.

The precision of estimating biological richness by lidar is currently unknown and still challenging to validate because the gold-standard (e.g., Malaise traps) are inconsistent as well.

The instrument limit of distinguishable species by entomological lidar is also unknown but the deployment of such a system at Ecuadorian sites is prone to provide this number statistically because the arthropod richness will include several thousand of species on a single site.

4. Conclusions and future work

We have successfully constructed a dual-band entomological lidar in Ecuador and tested it in a field campaign under particularly challenging atmospheric conditions, unlike any other previous lidar study. A hard target could be observed at a 2929 m range on rare occasions. Insects and vertebrates were observed easily up to 200 m distance and sampled at 5 kHz in a shared dual-band multiplexing scheme. While intensity domain thresholds yield rather low contrasts for insects embedded in the fog, in the frequency domain the contrast can be substantially higher. Thus, frequency domain thresholding may be advisable for detecting insects inside a fog. The combination of dense fog and large insects can cause oscillatory lidar extinction effects which are displayed in this work for the first time. The applications are yet to be explored, but the effect could enable independent estimation of geometrical cross-section and absolute spectral reflectance. We demonstrated a case where left- and right-wing movements induced oscillations in both intensity and the pixel spread and we could also associate features of the same signal with both the dorsal and ventral side of the wings by estimating melanization with the dual-band lidar.

Some considerations for future improvement can be also indicated. The employed receiver focal length is somewhat excessive and suboptimal for short ranges up to several hundred meters, which would be enough to profile through a virgin forest canopy even at an elevation angle. The long focal length also implies a high sensor tilt angle whereby the camera enclosure partly shades the Newtonian F/4 light cone impinging on the furthest pixels. The combination of a weaker laser at 980 nm and an inferior spectral response of the line camera at this band make the 980 nm signal one order of magnitude weaker than the 808 nm signal. The melanization effect of insects looking brighter at 980 nm only improves this unbalance marginally. Stronger 980 nm laser diodes with equivalent aperture are now available, however. The insect activity during our present dataset was relatively low compared to previous studies[16,23,24,35]. This is presumably both because the busy crepuscular rush hours were missed and because laser light was extinguished shortly after the system near limit most of the time. The latter issue can be fixed by a shorter receiver focal length.

The deployment of a dual-band entomological lidar in a region with one of the highest biodiversities in the world paves the way for beating several records over a global comparison: who can retrieve the largest number of distinct signals? Who can count most insects per cubic meter and time unit? What is the chronobiology of bat and bird insectivores in relation to their prey? How are the abundance and species richness stratified throughout the canopy heights? How to make robust data pipelines and benchmark this biodiversity assessment tool for the ultimate goal of better sustainable preservation and management of our planet?

Acknowledgments

The Ecuadorian entomological lidar instrument development and test were financed by CEDIA with a CEPRA XII Project. We greatly appreciate our host and cook Christophe Pellet for accommodation and for allowing us to work on his property (Bosque privado, Jardín de los Sueños, Maná, Ecuador). JS and MB's participation in this study was partly supported by the European Research Council (ERC) under the European Union's Horizon 2020 research and innovation program (grant agreement No. 850463). We thank Andrea Caicedo, José Tinajero

and Nicolas Tinoco from Pontificia Universidad Católica del Ecuador for participating in biological aspects of the field campaign. We thank Camilo Díaz, Elizabeth Samaniego and Iván De la Cruz from Escuela Politécnica Nacional for their collaboration during the entire project and fieldwork. We appreciate fruitful discussions with Samuel Jansson, Meng Li, Igor Buzuk, Eric Warrant, Jadranka Rota, David Dreyer, and Hampus Månefjord. This work was partially delayed due to the pandemic situation in Ecuador.

Disclosures

The authors declare that there are no conflicts of interest related to this article.

References

[1] D. S. Karp and G. C. Daily, "Cascading effects of insectivorous birds and bats in tropical coffee plantations," *Ecology,* vol. 95, pp. 1065-1074, 2014.

[2] B. A. Hawkins, R. Field, H. V. Cornell, D. J. Currie, J.-F. Guégan, D. M. Kaufman, J. T. Kerr, G. G. Mittelbach, T. Oberdorff, and E. M. O'Brien, "Energy, water, and broad‐scale geographic patterns of species richness," *Ecology,* vol. 84, pp. 3105-3117, 2003.

[3] C. Rahbek and G. R. Graves, "Multiscale assessment of patterns of avian species richness," *Proceedings of the National Academy of Sciences,* vol. 98, pp. 4534-4539, 2001.

[4] A. Balmford, K. J. Gaston, and A. James, "Integrating costs of conservation into international priority setting," *Conservation Biology,* vol. 14, pp. 597-605, 2000.

[5] D. de Souza Amorim, B. V. Brown, D. Boscolo, R. Ale-Rocha, D. M. Alvarez-Garcia, M. I. Balbi, A. de Marco Barbosa, R. S. Capellari, C. J. B. de Carvalho, and M. S. Couri, "Vertical stratification of insect abundance and species richness in an Amazonian tropical forest," *Scientific reports,* vol. 12, pp. 1-10, 2022.

[6] O. Dangles, Á. Barragán, R. E. Cárdenas, G. Onore, and C. Keil, "Entomology in Ecuador: Recent developments and future challenges," in *Annales de la Société entomologique de France*, 2009, pp. 424-436.

[7] O. Missa, Y. Basset, A. Alonso, S. E. Miller, G. Curletti, M. De Meyer, C. Eardley, M. W. Mansell, and T. Wagner, "Monitoring arthropods in a tropical landscape: relative effects of sampling methods and habitat types on trap catches," *Journal of Insect conservation,* vol. 13, pp. 103-118, 2009.

[8] P. J. DeVRIES, T. R. WALLA, and H. F. Greeney, "Species diversity in spatial and temporal dimensions of fruit-feeding butterflies from two Ecuadorian rainforests," *Biological Journal of the Linnean Society,* vol. 68, pp. 333-353, 1999.

[9] Y. Basset, L. Cizek, P. Cuénoud, R. K. Didham, V. Novotny, F. Ødegaard, T. Roslin, A. K. Tishechkin, J. Schmidl, N. N. Winchester, D. W. Roubik, H.-P. Aberlenc, J. Bail, H. Barrios, J. R. Bridle, G. Castaño-Meneses, B. Corbara, G. Curletti, W. Duarte da Rocha, D. De Bakker, J. H. C. Delabie, A. Dejean, L. L. Fagan, A. Floren, R. L. Kitching, E. Medianero, E. Gama de Oliveira, J. Orivel, M. Pollet, M. Rapp, S. P. Ribeiro, Y. Roisin, J. B. Schmidt, L. Sørensen, T. M. Lewinsohn, and M. Leponce, "Arthropod Distribution in a Tropical Rainforest: Tackling a Four Dimensional Puzzle," *PLOS ONE,* vol. 10, p. e0144110, 2015.

[10] Y. Basset, L. Cizek, P. Cuénoud, R. K. Didham, F. Guilhaumon, O. Missa, V. Novotny, F. Ødegaard, T. Roslin, and J. Schmidl, "Arthropod diversity in a tropical forest," *Science,* vol. 338, pp. 1481-1484, 2012.

[11] C. S. Svenningsen, T. G. Frøslev, J. Bladt, L. B. Pedersen, J. C. Larsen, R. Ejrnæs, C. Fløjgaard, A. J. Hansen, J. Heilmann-Clausen, and R. R. Dunn, "Detecting flying insects using car nets and DNA metabarcoding," *Biology Letters,* vol. 17, p. 20200833, 2021.

[12] A. M. Piper, J. Batovska, N. O. Cogan, J. Weiss, J. P. Cunningham, B. C. Rodoni, and M. J. Blacket, "Prospects and challenges of implementing DNA metabarcoding for high-throughput insect surveillance," *GigaScience,* vol. 8, p. giz092, 2019.

[13] B. L. Long, A. Kurta, and D. L. Clemans, "Analysis of DNA from feces to identify prey of Big Brown Bats (Eptesicus fuscus) caught in apple orchards," *The American Midland Naturalist,* vol. 170, pp. 287-297, 2013.

[14] L. Wührl, C. Pylatiuk, M. Giersch, F. Lapp, T. von Rintelen, M. Balke, S. Schmidt, P. Cerretti, and R. Meier, "DiversityScanner: Robotic handling of small invertebrates with machine learning methods," *Molecular ecology resources,* vol. 22, pp. 1626-1638, 2022.

[15] M. Brydegaard and S. Svanberg, "Photonic Monitoring of Atmospheric and Aquatic Fauna," *Laser & Photonics Reviews,* p. 1800135, 2018.

[16] B. K. Kouakou, S. Jansson, M. Brydegaard, and J. T. Zoueu, "Entomological Scheimpflug lidar for estimating unique insect classes in-situ field test from Ivory Coast," *OSA Continuum,* vol. 3, pp. 2362-2371, 2020/09/15 2020.

[17] K. Rydhmer, E. Bick, L. Still, A. Strand, R. Luciano, S. Helmreich, B. D. Beck, C. Grønne, L. Malmros, K. Poulsen, F. Elbæk, M. Brydegaaard, J. Lemmich, and T. Nikolajsen, "Automating insect monitoring using unsupervised near-infrared sensors," *Scientific Reports,* vol. 12, pp. 1-11, 2022.

[18] T. T. Høye, J. Ärje, K. Bjerge, O. L. Hansen, A. Iosifidis, F. Leese, H. M. Mann, K. Meissner, C. Melvad, and J. Raitoharju, "Deep learning and computer vision will transform entomology," *Proceedings of the National Academy of Sciences,* vol. 118, 2021.

[19] M. Brydegaard, A. Gebru, and S. Svanberg, "Super resolution laser radar with blinking atmospheric particles – application to interacting flying insects.," *Prog. Electromagn. Res.,* vol. 147, pp. 141-151, 2014.

[20] L. Mei and M. Brydegaard, "Atmospheric aerosol monitoring by an elastic Scheimpflug lidar system," *Optics Express,* vol. 23, pp. A1613-A1628, 2015.

[21] M. Brydegaard, E. Malmqvist, S. Jansson, J. Larsson, S. Török, and G. Zhao, "The Scheimpflug Lidar Method," *SPIE Lidar Remote Sensing for Environmental Monitoring,* vol. 10406, 2017.

[22] E. Malmqvist, M. Brydegaard, M. Aaldén, and J. Bood, "Scheimpflug Lidar for combustion diagnostics," *Optics Express,* 2018.

[23] S. Jansson, E. Malmqvist, Y. Mlacha, R. Ignell, F. Okumu, G. Killeen, C. Kirkeby, and M. Brydegaard, "Real-time dispersal of malaria vectors in rural Africa monitored with lidar," *PLoS One,* 2020.

[24] E. Malmqvist, S. Jansson, S. Zhu, W. Li, K. Svanberg, S. Svanberg, J. Rydell, Z. Song, J. Bood, M. Brydegaard, and S. Åkesson, "The bat-bird-bug battle: daily flight activity of insects and their predators over a rice field revealed by high resolution Scheimpflug Lidar " *Royal Society Open Science,* vol. 5, 2018.

[25] Y. Li, K. Wang, R. Quintero-Torres, R. Brick, A. V. Sokolov, and M. O. Scully, "Insect flight velocity measurement with a CW near-IR Scheimpflug lidar system," *Optics Express,* vol. 28, pp. 21891-21902, 2020/07/20 2020.

[26] K. Rydhmer, J. Prangsma, M. Brydegaard, H. Smith, C. Kirkeby, I. K. Schmidt, and B. Boelt, "Lidar profiling of bee activity patterns and foraging distributions," *Animal Telemetry,* 2022.

[27] G. Zhao, E. Malmqvist, S. Török, P.-E. Bengtsson, S. Svanberg, J. Bood, and M. Brydegaard, "Particle profiling and classification by a dual-band continuous-wave lidar system," *Applied optics,* vol. 57, pp. 10164-10171, 2018.

[28] S. Zhu, E. Malmqvist, W. Li, S. Jansson, Y. Li, Z. Duan, K. Svanberg, H. Feng, Z. Song, G. Zhao, M. Brydegaard, and S. Svanberg, "Insect abundance over Chinese rice fields in relation to environmental parameters, studied with a polarization-sensitive CW near-IR lidar system," *Applied Physics B,* vol. 123, 2017.

[29] L. Mei and P. Guan, "Development of an atmospheric polarization Scheimpflug lidar system based on a time-division multiplexing scheme," *Optics Letters,* vol. 42, pp. 3562-3565, 2017/09/15 2017.

[30] H. Yin, L. Shi, J. Sha, Y. Li, Y. Qin, B. Dong, S. Meyer, X. Liu, L. Zhao, and J. Zi, "Iridescence in the neck feathers of domestic pigeons," *Phys. Rev. E,* vol. 74, p. 051916, 2006.

[31] M. Li, C. Seinsche, S. Jansson, J. Hernandez, J. Rota, E. Warrant, and M. Brydegaard, "Potential for identification of wild night-flying moths by remote infrared microscopy " *Royal Society Interface,* 2022.

[32] M. Li, S. Jansson, A. Runemark, J. Peterson, C. Kirkeby, A. M. Jönsson, and M. Brydegaard, "Bark beetles as lidar targets and prospects of photonic surveillance," *Journal of Biophotonics,* 2020.

[33] M. Brydegaard, S. Jansson, M. Schulz, and A. Runemark, "Can the narrow red bands of dragonflies be used to perceive wing interference patterns?," *Ecology and evolution,* vol. 8, pp. 5369-5384, 2018.

[34] M. Brydegaard, "Towards quantitative optical cross sections in entomological laser radar – Potential of temporal and spherical parameterizations for identifying atmospheric fauna," *PLoS One,* vol. 10, p. e0135231, 2015.

[35] M. Brydegaard, B. Kouakou, S. Jansson, J. Rydell, and J. Zoueu, "High Dynamic Range in Entomological Scheimpflug Lidars," *IEEE Journal of Selected Topics in Quantum Electronics,* 2021.

[36] S. Jansson, E. Malmqvist, M. Brydegaard, S. Åkesson, and J. Rydell, "A Scheimpflug lidar used to observe insect swarming at a wind turbine," *Ecological Indicators,* vol. 117, p. 106578, 2020.

[37] A. Gebru, S. Jansson, R. Ignell, C. Kirkeby, J. Prangsma, and M. Brydegaard, "Multiband modulation spectroscopy for determination of sex and species of mosquitoes in flight," *J. Biophotonics,* vol. 11, 2018.

[38] A. P. Genoud, R. Basistyy, G. M. Williams, and B. P. Thomas, "Optical remote sensing for monitoring flying mosquitoes, gender identification and discussion on species identification," *Applied Physics B,* vol. 124, p. 46, February 17 2018.

[39] M. Sikulu, G. F. Killeen, L. E. Hugo, P. A. Ryan, K. M. Dowell, R. A. Wirtz, S. J. Moore, and F. E. Dowell, "Near-infrared spectroscopy as a complementary age grading and species identification tool for African malaria vectors," *Parasit. Vectors,* vol. 3, p. 49, 2010.

[40] A. P. Hill, P. Prince, E. Piña Covarrubias, C. P. Doncaster, J. L. Snaddon, and A. Rogers, "AudioMoth: Evaluation of a smart open acoustic device for monitoring biodiversity and the environment," *Methods in Ecology and Evolution,* vol. 9, pp. 1199-1211, 2018.

[41] P. Jancovic and M. Köküer, "Bird species recognition using unsupervised modeling of individual vocalization elements," *IEEE/ACM Transactions on Audio, Speech, and Language Processing,* vol. 27, pp. 932-947, 2019.

Dual-band infrared Scheimpflug lidar reveals insect activity in a tropical cloud forest

VICTOR SANTOS[1], CESAR COSTA-VERA[1*], PAMELA RIVERA-PARRA[2], SANTIAGO BURNEO[3], JUAN MOLINA[1], DIANA ENCALADA[4], JACOBO SALVADOR[5], AND MIKKEL BRYDEGAARD[5,6]

[1]*Dpto. de Física, Escuela Politécnica Nacional, Av. Ladrón de Guevara E11-253, Quito 170525, Ecuador*

[2]*Dpto. de Biología, Escuela Politécnica Nacional, Av. Ladrón de Guevara E11-253, Quito 170525, Ecuador*

[3]*Pontificia Universidad Católica del Ecuador, Avenida 12 de Octubre 1076, Quito*

[4]*Dpto. de Economía, Universidad Técnica Particular de Loja, San Cayetano Alto, Loja, Ecuador*

[5]*Dept. of Physics, Lund University, Sölvegatan 14c, 22362 Lund, Sweden*

[6]*Norsk Elektro Optikk AS, Østensjøveien 34, 0667 Oslo, Norway*

**cesar.costa@epn.edu.ec*

Abstract

We describe an entomological dual-band 808 and 980 nm lidar system which has been implemented in a tropical cloud forest (Ecuador). The system was successfully tested at a sample rate of 5 kHz in a cloud forest during challenging foggy conditions (extinction coefficients of 20 km^{-1} under good

light transmission conditions) for the first time. At times, the backscattered signal could be retrieved from a distance of 2929 m. We present insect and bat observations up to 200 m during a single night with an emphasis on fog aspects, potentials, and benefits of such dual-band systems. We demonstrate that the modulation contrast between insects and fog is high in the frequency domain compared to intensity in the time domain, thus allowing for better identification and quantification in misty forests. Oscillatory lidar extinction effects are shown in this work for the first time, caused by the combination of dense fog and large moths partially obstructing the beam. We demonstrate here an interesting case of a moth where left- and right-wing movements induced oscillations in both intensity and pixel spread. In addition, we were able to identify the dorsal and ventral sides of the wings by estimating the corresponding melanization with the dual-band lidar. We demonstrate that the wing beat trajectories in the dual-band parameter space are complementary rather than covarying or redundant, thus dual-band entomological lidar approach to biodiversity studies is feasible *in situ* and endows species specificity differentiation. Future improvements are discussed. The introduction of these methodologies opens the door to a wealth of possible experiments to monitor, understand and safeguard the biological resources of one of the most biodiverse countries on earth.

Keywords

Scheimplufg Light Detection and Ranging, Entomological Sensor, Dual-Band Ranger, Insect Activity, Foggy Conditions, Frequency Domain.

INTRODUCTION

Assessment of biodiversity is fundamental for understanding complex interactions[1] and for preserving ecosystems. Factors such as rainfall, mountainous topography, and vicinity to the equator all increase species richness[2,3] of trees, birds, mammals, reptiles, amphibians, and insects. Unfortunately, many important biodiversity hotspots, such as Andean tropical rainforests, remain poorly studied[4]. Species inventorying in a tall standing rainforest is challenging; vegetation and dense fog limit visibility and insect species are vertically stratified[5]. Conventional surveys include traps and sweepnets[6], but generally, traps and baits are biased[7] and limit studies to subgroups of species. As an example, hundreds of species of fruit-feeding butterflies can be found at a single Ecuadorian site, but are insufficiently identifiable by this approach[8]. More general estimations of insect species in the richness of tropical virgin forests are costly and complicated[9,10]. Analysis of caught samples may also be exceedingly laborious. Metabarcoding can detect the presence of species in genetic

databases[11-13] but fail to report on abundances. Innovative solutions with machine vision and robotics may be required to automate catch analysis[14].

Photonic monitoring approaches[15-18] may be able to estimate the insect species richness in real-time *in situ*, without biasing, sample handling, or great collecting efforts. Furthermore, entomological lidar could access diversity throughout tall canopies of virgin forests, which are known to foster higher diversity.

The aim of this paper is to present a novel dual-band (808 and 980 nm) entomological lidar in Ecuador. In particular, we showcase the feasibility of remotely observing insects *in situ* during severely foggy conditions (with attenuation coefficient of 20 km^{-1} in pristine air conditions) for the first time and demonstrate how two bands provide complementary information and can be expected to distinguish more species.

[Insert Figure 1.]

METHODS

Field site

The study was carried out in the private reserve "Bosque Protector Jardín de los Sueños", an evergreen forest (~500 m asl) at the foot of the western Andean ridge in Cotopaxi province, Ecuador. The entomological lidar system introduced in this work and its main components are presented in Fig.1. The instrument is shown overlooking the interrogation volume in the reserve. In this geographical location, the annual mean temperatures are 18-24 °C with a mean

relative humidity of 86%. There is an average rainfall of 7 m/year, and the dry season extends between July and December, while the rainy season goes from January to May. This mountainous forest is part of the remaining Chocó rainforest region which covers most of Colombia's Pacific coast. The location presents fog and mist through most of the day all year around. The forest includes primary virgin vegetation with tree canopies above 50 m (Fig.2d) and some secondary forest at the edges. The site is a biodiversity hotspot and hosts a broad range of animal species on the ground, throughout the canopy, and free-flying. Because of this and other factors, this reserve has been identified as an important wildlife refuge for all taxonomic groups, with a special emphasis on bats. In the year 2021, the reserve was designated as an important preservation spot by the Ecuadorian Bat Conservation Program. This location provides an interesting place to study bat-prey interactions. Forest patches such as this act as a biodiversity source for the surrounding territories and is a crucial fountain of ecosystem services such as pollination, seed dispersal, and refuge for pest predators.

Test range

For the feasibility test, the lidar system was transported to the field site and mounted in an open-side garage tent (Fig.1a, 0°50'15.30"S, 79°12'18.64"W). The system was powered with a 2 kW generator placed at about 25 m in distance. The lidar was overlooking a descending skirt toward a valley covered by forest. This work reports results obtained from a transect terminating in a

coffee plantation (Fig.2d. 0°50'54.92"S, 79°13'44.17"W), some 2950 m from the lidar. In its path, the beam descended at 4.5° from 577 m to 346 m asl (Fig.2c). Around 800 m, the beam was surrounded by tall canopies on both sides (Fig.2e).

[Insert Figure 2.]

Dual-band entomological lidar

The developed entomological lidar was designed according to the Scheimpflug lidar principle[19-22]. This method employs multiplexed continuous wave lasers and triangulation in combination with the Scheimpflug focus strategy whereby sharp focus can be accomplished at all distances simultaneously despite the use of large apertures. This, in turn, allows for fast acquisition up to several kHz and capturing of the oscillatory properties of non-stationary insect targets[16,23]. Our system resembles previous systems on other continents[16,24-26], and it also consists of a transmitter and a receiver mounted on an aluminum baseline frame with an 845 mm separation (see Fig.1a and Fig.3). This baseline is in turn, mounted on a heavy-duty motorized tripod (EQ8, SkyWatcher, China) for stable positioning and pointing. The transmitter is comprised of a beam expander with Ø120mm/f600mm, (Startravel 120OTA, SkyWatcher, China) with an upgraded focal stage (Monorail R96, Teleskop Service, Germany). A dichroic beam splitter (Fig.3a) is installed on a rotary stage at the focal port of the beam expander (#69-907, Edmund Optics, USA with B4CRP/M, Thorlabs, USA). Two c-mount diode lasers are installed on the branches of the beam

splitter: a 5W, 808 nm diode, and a 3W, 980 nm diode (MLD-808-5000 and MLD-980-3000, CNI laser, China). Both beams are TM polarized with an aperture of 100 µm and rod lenses for matching the divergences. TM polarization implies that the E-field is parallel to the baseline of the lidar. The diodes are ordered with a Fast Axis Collimating lens precision glued to the device. Hereby divergence is 8° in both axes, and the collection efficiency by the F/5 telescope becomes 82%. The laser beam splitter mounting stage allows for a precise super-positioning of the two sources, while a cage system mounting permits the relative focus adjustment of the two diodes to compensate for the achromatic focal shift of the expander. For lidar overlap purposes, the beam expander is mounted on the baseline with a tangential mount (Stronghold, Baader, Germany).

The receiver is a Ø250mm/f1000mm Newtonian reflecting telescope (Quattro-10S, SkyWatcher, China). A custom wedge is installed in the focal port. This wedge holds a ø50mm RG780 long pass filter (Edmund Optics, USA). Further, the wedge supports a linear CMOS camera (OctoPlus EV71YO1CUB2210-BB1, Teledyne e2v Imaging, USA). This 12-bit USB3 camera has 2048 pixels of 10×200µm each and can reach line rates of 80 kHz. The camera emits a kHz strobe pulse at every exposure, this signal is used to alternate the laser driver between 3 states: dark, 808 nm and 980 nm (see Fig.3b). This lock-in multiplexing method is also described in previous work[27-29]. Light interaction with insects in the NIR region is dominated by melanization

and thinfilm[30] effects. Fig.3c displays the band placement in relation to typical melanization of insects[31]. Fig.3d displays the ability of the two bands to produce resonant backscatter depending on the wing thickness for typical insect wing thicknesses[32,33]. The entomological lidar is a non-invasive technique, meant to capture the natural behavior of insects *in situ* and real-time. For this, laser beams that are invisible to insects must be used when possible. On the one hand, from 800 nm to longer wavelengths in the near infrared, this is predominantly true. On the other hand, fast Scheimpflug lidars are based on linear Si CMOS arrays with kHz rate readout. The bandgap of these detectors allows detecting photons up to 1000 nm in wavelength. Within this spectral range, to retrieve complementary information from the target, a sensible strategy involves using multiple interrogation bands. The insect features which could cause a differential response within this range would be a) absorption by the biopolymer melanin, and b) thin film interference effects from the ½-3 μm-thick (and smaller) chitin structures in the wing membranes. None of the generated spectral features are particularly sharp, therefore a wide as possible wavelength separation is desirable. Fig.3c-d shows our solution for this. As there are only a handful of diode laser bands in this range, we elected lasers emitting in the 808 nm and 980 nm bands, that are more common and efficient than others.

Finally, the lidar is equipped with an additional refracting telescope Ø102mm/f500mm (StarTravel, SkyWatcher, China) with a NIR sensitive USB3 camera (acA1920-155um, Bassler, Germany) for surveillance and beam alignment purpose (see Fig.2e). All telescopes are fitted with anti-dew bands to prevent water condensation on the optics (Astroshop, Germany). A complete components list is available from the corresponding author upon request.

[Insert Figure 3.]

System operation and data collection

The system is operated from an adjacent laptop. The computer produces a preview of the infrared monitor camera for beam alignment purposes. The actual lidar data acquisition is done by a custom-made, real-time, user interface programmed in LabView (National Instruments, USA). The program was set to capture frames of 30000 exposures × 2048 pixels, it then demultiplexes the frame into a 3D tensor of 10000 exposures × 2048-pixel × 3 time slots (dark/808nm/980nm). The dark timeslot is identified by its minimum average total intensity and is subtracted from the 808 and 980 nm timeslot. The program then displays the minimum/median / maximum pixel profile (range echo) for each band. Also, the dark signal is displayed in a separate graph. The graphs update every time a new frame is acquired and 12bit raw intensity data is continuously saved at an external USB3 drive. Each filename is time stamped and each frame file is 120 Mb. In this work the line rate was set to 5 kHz, line

period 200 µs, exposure time 180 µs, pre-amplifier 4x, gain 8x, and bias 0 counts.

RESULTS

Our report from this initial work focuses on the detection of insects under a dense fog, which is particularly relevant for monitoring the biodiversity of cloud forests under real natural conditions. In Fig.4a, the first light of the Ecuadorian lidar is presented in a time-range map displaying the first half hour of the measurements. The color coding includes the max signal from both bands as well as the median from the 808 nm band. Insects show up as green dots, bats are seen as yellow dots while the fog is identifiable in shades of blue and white. Artifacts from fireflies are also seen on some occasions. Initially, back-scattered light is retrieved over the full range of 3 km, the fog then closes in and extinguishes light after 100 m. The plot is made from 250 lidar files, each spanning 6 s. In Fig.4b we display the time and range resolved frequency content in a single file. Even though the fog is much stronger in backscatter compared to insects, the frequency content of fog is relatively low. This implies that it may be challenging to contrast out insects inside fog in the intensity-time domain while the contrast in the power-frequency domain is much higher.

[Insert Figure 4.]

In Fig.5 we highlight the first insect observation at 90 m of distance during 200 ms (same file as Fig.4b). The signal from the insect is small compared to

the fog layer at 300 m distance, still the fog is thin enough at this point that allows light to reach the termination at 3 km and return. Fig.5b also shows that the 980 nm signal is one order of magnitude weaker than the 808 nm band. There are multiple reasons for this: 1) weaker laser power, 2) worse spectral response of the detector, and 3) less atmospheric scattering. The echo of the insect is, however, stronger for the 980 nm band, relative to the atmospheric signal. This is because melanin absorbs less in the 980 nm band (See Fig.3c). If the system was white calibrated against a target with flat spectral reflectance, the band ratio from the body signal would be converted into the equivalent absorption path length of pure melanin in microns[31]. For the wing signal this is slightly more complicated since clear wings produce thin film fringes[32,33] (see Fig.3d). Also, the body- and wing signals can be seen in the time domain, as shown in Fig.5c, as a bias envelope and an oscillatory part, respectively. A close inspection of the signal also demonstrates a highly periodic waveform with various features. The frequency content of the signals in Fig.5d indicates a wing beat frequency of 136 Hz. The 100-200 Hz range is a common wingbeat frequency among insects[16,23,32,34], such as flies and beetles, thus we could not make more informed guesses about the family it belongs to, except that we are dealing with a clear-winged insect (not a moth) because of the spiky waveform and the numerous harmonics. This case also demonstrates that the second harmonic is often stronger than the fundamental tone which can be a challenge for a prospective automatic pitch detection[23].

[Insert Figure 5.]

The case highlighted in Fig.6 is instead a moth. This is supported by the hour of flight, the rather low wingbeat frequency, the smooth waveform (low-intensity skewness), and the large apparent size[24,35,36] of 84 mm. Detailed inspection of the signal in Fig.6a reveals a particular dynamics not only in intensity but also in the pixel spread value, the pattern can be explained by scattering contributions from both the dorsal and ventral sides of the left and right wings of the insect. Fig.6a also reveals for the first time oscillatory lidar extinction, where the fog backscatter beyond the moth is shaded when the wings display maximal cross-section. In Fig.6b, the range echoes for each of the two bands are displayed at the times t_{fog} and t_{moth} indicated in Fig.6a. Signal reduction beyond the moth is seen. In theory, lidars can acquire both backscatter and extinction cross sections, and in the applications for entomological lidars is possible to determine both the geometrical cross section and the reflectance at specific bands independently. At this time of the night, laser light was extinguished after 200 m, for guidance exponential decays (round-trip) are superimposed on the graphs in Fig.6b. In this case the moth is detected during extremely dense fog conditions with an attenuation coefficient, μ_{att}, in the order of 20 km^{-1}, as obtained from the underlying exponential fitting.

[Insert Figure 6.]

The benefits of dual-band[37,38] and hyperspectral[39] detection of insects have previously been demonstrated in laboratory settings. In Fig.7 we show that the two spectral bands contribute complementary information and that they are not simply redundant. To support this, consider that the correlation of the two bands in Fig.7. is 72% demonstrating that they are not completely redundant but, rather, complementary (they should have been 100% correlated otherwise). If we neglect the noise, this result implies that adding the second band contributes 28% of new information. This value could obviously be greater or smaller for other species. Also, it is evident, that the signals in the 808 and 980 nm bands are far from co-varying throughout the ~4 wingbeats seen in Fig.6. The trajectory in the spectral parameter plane in Fig.7 is color-coded by the time during transit. Several repeated features can be observed; straight and fast down strokes, wavy slow upstrokes, a secondary minor peak from the right wing, and a counterclockwise pattern due to contributions from both the melanized dorsal side and the brighter ventral side[31]. The dual-band information retrieved is indeed rich much beyond the simple modulation power spectra in Fig.6, and thus the potential of applying this complementarity to differentiate numerous species is promising. To date, there are well-established methods for signal diversity assessment, deriving from scientific communities of music analysis, speech recognition, and bioacoustics[40,41]. Unfortunately, most audio approaches are insensitive to waveforms and relative phases of harmonics. The

concept of including multiple bands and polarizations waveforms in diversity computations is even more exotic in this literature.

[Insert Figure 7.]

The precision of estimating biological richness by lidar is currently unknown and still challenging to validate because the gold-standard (e.g., Malaise traps) are inconsistent as well. The instrument limit of distinguishable species by entomological lidar is also unknown but the deployment of such a system at Ecuadorian sites is prone to provide this number statistically because the arthropod richness will include several thousand of species on a single site.

CONCLUSIONS AND FUTURE WORK

We have successfully constructed a dual-band entomological lidar in Ecuador and tested it in a field campaign under particularly challenging atmospheric conditions, unlike any other previous lidar study. A hard target could be observed at a 2929 m range on rare occasions. Insects and vertebrates were observed easily up to 200 m distance and sampled at 5 kHz in a shared dual-band multiplexing scheme. While intensity domain thresholds yield rather low contrasts for insects embedded in the fog, in the frequency domain the contrast can be substantially higher. Thus, frequency domain thresholding may be advisable for detecting insects inside a fog. The combination of dense fog and large insects can cause oscillatory lidar extinction effects which are displayed in this work for the first time. The applications are yet to be explored, but the

effect could enable independent estimation of geometrical cross-section and absolute spectral reflectance. We demonstrated a case where left- and right-wing movements induced oscillations in both intensity and the pixel spread and we could also associate features of the same signal with both the dorsal and ventral side of the wings by estimating melanization with the dual-band lidar.

Some considerations for future improvement can be also indicated. The employed receiver focal length is somewhat excessive and suboptimal for short ranges up to several hundred meters, which would be enough to profile through a virgin forest canopy even at an elevation angle. The long focal length also implies a high sensor tilt angle whereby the camera enclosure partly shades the Newtonian F/4 light cone impinging on the furthest pixels. The combination of a weaker laser at 980 nm and an inferior spectral response of the line camera at this band make the 980 nm signal one order of magnitude weaker than the 808 nm signal. The melanization effect of insects looking brighter at 980 nm only improves this unbalance marginally. Stronger 980 nm laser diodes with equivalent aperture are now available, however. The insect activity during our present dataset was relatively low compared to previous studies[16,23,24,35]. This is presumably both because the busy crepuscular rush hours were missed and because laser light was extinguished shortly after the system near limit most of the time. The latter issue can be fixed by a shorter receiver focal length.

The deployment of a dual-band entomological lidar in a region with one of the highest biodiversities in the world paves the way for beating several records

over a global comparison: who can retrieve the largest number of distinct signals? Who can count most insects per cubic meter and time unit? What is the chronobiology of bat and bird insectivores in relation to their prey? How are the abundance and species richness stratified throughout the canopy heights? How to make robust data pipelines and benchmark this biodiversity assessment tool for the ultimate goal of better sustainable preservation and management of our planet?

Acknowledgments

The Ecuadorian entomological lidar instrument development and test were financed by CEDIA with a CEPRA XII Project. We greatly appreciate our host and cook Christophe Pellet for accommodation and for allowing us to work on his property (Bosque privado, Jardín de los Sueños, Maná, Ecuador). JS and MB's participation in this study was partly supported by the European Research Council (ERC) under the European Union's Horizon 2020 research and innovation program (grant agreement No. 850463). We thank Andrea Caicedo, José Tinajero and Nicolas Tinoco from Pontificia Universidad Católica del Ecuador for participating in biological aspects of the field campaign. We thank Camilo Díaz, Elizabeth Samaniego and Iván De la Cruz from Escuela Politécnica Nacional for their collaboration during the entire project and fieldwork. We appreciate fruitful discussions with Samuel Jansson, Meng Li, Igor Buzuk, Eric Warrant, Jadranka Rota, David Dreyer, and Hampus

Månefjord. This work was partially delayed due to the pandemic situation in Ecuador.

Disclosures

The authors declare that there are no conflicts of interest related to this article.

References

1. D. S. Karp and G. C. Daily, "Cascading effects of insectivorous birds and bats in tropical coffee plantations," *Ecology,* vol. 95, pp. 1065-1074, 2014.
2. B. A. Hawkins, R. Field, H. V. Cornell, D. J. Currie, J.-F. Guégan, D. M. Kaufman, J. T. Kerr, G. G. Mittelbach, T. Oberdorff, and E. M. O'Brien, "Energy, water, and broad-scale geographic patterns of species richness," *Ecology,* vol. 84, pp. 3105-3117, 2003.
3. C. Rahbek and G. R. Graves, "Multiscale assessment of patterns of avian species richness," *Proceedings of the National Academy of Sciences,* vol. 98, pp. 4534-4539, 2001.
4. A. Balmford, K. J. Gaston, and A. James, "Integrating costs of conservation into international priority setting," *Conservation Biology,* vol. 14, pp. 597-605, 2000.
5. D. de Souza Amorim, B. V. Brown, D. Boscolo, R. Ale-Rocha, D. M. Alvarez-Garcia, M. I. Balbi, A. de Marco Barbosa, R. S. Capellari, C. J. B. de Carvalho, and M. S. Couri, "Vertical stratification of insect

abundance and species richness in an Amazonian tropical forest," *Scientific reports,* vol. 12, pp. 1-10, 2022.

6. O. Dangles, Á. Barragán, R. E. Cárdenas, G. Onore, and C. Keil, "Entomology in Ecuador: Recent developments and future challenges," in *Annales de la Société entomologique de France*, 2009, pp. 424-436.
7. O. Missa, Y. Basset, A. Alonso, S. E. Miller, G. Curletti, M. De Meyer, C. Eardley, M. W. Mansell, and T. Wagner, "Monitoring arthropods in a tropical landscape: relative effects of sampling methods and habitat types on trap catches," *Journal of Insect conservation,* vol. 13, pp. 103-118, 2009.
8. P. J. DeVRIES, T. R. WALLA, and H. F. Greeney, "Species diversity in spatial and temporal dimensions of fruit-feeding butterflies from two Ecuadorian rainforests," *Biological Journal of the Linnean Society,* vol. 68, pp. 333-353, 1999.
9. Y. Basset, L. Cizek, P. Cuénoud, R. K. Didham, V. Novotny, F. Ødegaard, T. Roslin, A. K. Tishechkin, J. Schmidl, N. N. Winchester, D. W. Roubik, H.-P. Aberlenc, J. Bail, H. Barrios, J. R. Bridle, G. Castaño-Meneses, B. Corbara, G. Curletti, W. Duarte da Rocha, D. De Bakker, J. H. C. Delabie, A. Dejean, L. L. Fagan, A. Floren, R. L. Kitching, E. Medianero, E. Gama de Oliveira, J. Orivel, M. Pollet, M. Rapp, S. P. Ribeiro, Y. Roisin, J. B. Schmidt, L. Sørensen, T. M.

Lewinsohn, and M. Leponce, “Arthropod Distribution in a Tropical Rainforest: Tackling a Four Dimensional Puzzle,” *PLOS ONE,* vol. 10, p. e0144110, 2015.

10. Y. Basset, L. Cizek, P. Cuénoud, R. K. Didham, F. Guilhaumon, O. Missa, V. Novotny, F. Ødegaard, T. Roslin, and J. Schmidl, “Arthropod diversity in a tropical forest,” *Science,* vol. 338, pp. 1481-1484, 2012.
11. C. S. Svenningsen, T. G. Frøslev, J. Bladt, L. B. Pedersen, J. C. Larsen, R. Ejrnæs, C. Fløjgaard, A. J. Hansen, J. Heilmann-Clausen, and R. R. Dunn, “Detecting flying insects using car nets and DNA metabarcoding,” *Biology Letters,* vol. 17, p. 20200833, 2021.
12. A. M. Piper, J. Batovska, N. O. Cogan, J. Weiss, J. P. Cunningham, B. C. Rodoni, and M. J. Blacket, “Prospects and challenges of implementing DNA metabarcoding for high-throughput insect surveillance,” *GigaScience,* vol. 8, p. giz092, 2019.
13. B. L. Long, A. Kurta, and D. L. Clemans, “Analysis of DNA from feces to identify prey of Big Brown Bats (Eptesicus fuscus) caught in apple orchards,” *The American Midland Naturalist,* vol. 170, pp. 287-297, 2013.
14. L. Wührl, C. Pylatiuk, M. Giersch, F. Lapp, T. von Rintelen, M. Balke, S. Schmidt, P. Cerretti, and R. Meier, “DiversityScanner:

Robotic handling of small invertebrates with machine learning methods," *Molecular ecology resources,* vol. 22, pp. 1626-1638, 2022.

15. M. Brydegaard and S. Svanberg, "Photonic Monitoring of Atmospheric and Aquatic Fauna," *Laser & Photonics Reviews,* p. 1800135, 2018.
16. B. K. Kouakou, S. Jansson, M. Brydegaard, and J. T. Zoueu, "Entomological Scheimpflug lidar for estimating unique insect classes in-situ field test from Ivory Coast," *OSA Continuum,* vol. 3, pp. 2362-2371, 2020/09/15 2020.
17. K. Rydhmer, E. Bick, L. Still, A. Strand, R. Luciano, S. Helmreich, B. D. Beck, C. Grønne, L. Malmros, K. Poulsen, F. Elbæk, M. Brydegaaard, J. Lemmich, and T. Nikolajsen, "Automating insect monitoring using unsupervised near-infrared sensors," *Scientific Reports,* vol. 12, pp. 1-11, 2022.
18. T. T. Høye, J. Ärje, K. Bjerge, O. L. Hansen, A. Iosifidis, F. Leese, H. M. Mann, K. Meissner, C. Melvad, and J. Raitoharju, "Deep learning and computer vision will transform entomology," *Proceedings of the National Academy of Sciences,* vol. 118, 2021.
19. M. Brydegaard, A. Gebru, and S. Svanberg, "Super resolution laser radar with blinking atmospheric particles – application to interacting flying insects.," *Prog. Electromagn. Res.,* vol. 147, pp. 141-151, 2014.

20. L. Mei and M. Brydegaard, "Atmospheric aerosol monitoring by an elastic Scheimpflug lidar system," *Optics Express,* vol. 23, pp. A1613-A1628, 2015.
21. M. Brydegaard, E. Malmqvist, S. Jansson, J. Larsson, S. Török, and G. Zhao, "The Scheimpflug Lidar Method," *SPIE Lidar Remote Sensing for Environmental Monitoring,* vol. 10406, 2017.
22. E. Malmqvist, M. Brydegaard, M. Aaldén, and J. Bood, "Scheimpflug Lidar for combustion diagnostics," *Optics Express,* 2018.
23. S. Jansson, E. Malmqvist, Y. Mlacha, R. Ignell, F. Okumu, G. Killeen, C. Kirkeby, and M. Brydegaard, "Real-time dispersal of malaria vectors in rural Africa monitored with lidar," *PLoS One,* 2020.
24. E. Malmqvist, S. Jansson, S. Zhu, W. Li, K. Svanberg, S. Svanberg, J. Rydell, Z. Song, J. Bood, M. Brydegaard, and S. Åkesson, "The bat-bird-bug battle: daily flight activity of insects and their predators over a rice field revealed by high resolution Scheimpflug Lidar " *Royal Society Open Science,* vol. 5, 2018.
25. Y. Li, K. Wang, R. Quintero-Torres, R. Brick, A. V. Sokolov, and M. O. Scully, "Insect flight velocity measurement with a CW near-IR Scheimpflug lidar system," *Optics Express,* vol. 28, pp. 21891-21902, 2020/07/20 2020.

26. K. Rydhmer, J. Prangsma, M. Brydegaard, H. Smith, C. Kirkeby, I. K. Schmidt, and B. Boelt, "Lidar profiling of bee activity patterns and foraging distributions," *Animal Telemetry,* 2022.

27. G. Zhao, E. Malmqvist, S. Török, P.-E. Bengtsson, S. Svanberg, J. Bood, and M. Brydegaard, "Particle profiling and classification by a dual-band continuous-wave lidar system," *Applied optics,* vol. 57, pp. 10164-10171, 2018.

28. S. Zhu, E. Malmqvist, W. Li, S. Jansson, Y. Li, Z. Duan, K. Svanberg, H. Feng, Z. Song, G. Zhao, M. Brydegaard, and S. Svanberg, "Insect abundance over Chinese rice fields in relation to environmental parameters, studied with a polarization-sensitive CW near-IR lidar system," *Applied Physics B,* vol. 123, 2017.

29. L. Mei and P. Guan, "Development of an atmospheric polarization Scheimpflug lidar system based on a time-division multiplexing scheme," *Optics Letters,* vol. 42, pp. 3562-3565, 2017/09/15 2017.

30. H. Yin, L. Shi, J. Sha, Y. Li, Y. Qin, B. Dong, S. Meyer, X. Liu, L. Zhao, and J. Zi, "Iridescence in the neck feathers of domestic pigeons," *Phys. Rev. E,* vol. 74, p. 051916, 2006.

31. M. Li, C. Seinsche, S. Jansson, J. Hernandez, J. Rota, E. Warrant, and M. Brydegaard, "Potential for identification of wild night-flying moths by remote infrared microscopy " *Royal Society Interface,* 2022.

32. M. Li, S. Jansson, A. Runemark, J. Peterson, C. Kirkeby, A. M. Jönsson, and M. Brydegaard, “Bark beetles as lidar targets and prospects of photonic surveillance,” *Journal of Biophotonics,* 2020.
33. M. Brydegaard, S. Jansson, M. Schulz, and A. Runemark, “Can the narrow red bands of dragonflies be used to perceive wing interference patterns?,” *Ecology and evolution,* vol. 8, pp. 5369-5384, 2018.
34. M. Brydegaard, “Towards quantitative optical cross sections in entomological laser radar – Potential of temporal and spherical parameterizations for identifying atmospheric fauna,” *PloS One,* vol. 10, p. e0135231, 2015.
35. M. Brydegaard, B. Kouakou, S. Jansson, J. Rydell, and J. Zoueu, “High Dynamic Range in Entomological Scheimpflug Lidars,” *IEEE Journal of Selected Topics in Quantum Electronics,* 2021.
36. S. Jansson, E. Malmqvist, M. Brydegaard, S. Åkesson, and J. Rydell, “A Scheimpflug lidar used to observe insect swarming at a wind turbine,” *Ecological Indicators,* vol. 117, p. 106578, 2020.
37. A. Gebru, S. Jansson, R. Ignell, C. Kirkeby, J. Prangsma, and M. Brydegaard, "Multiband modulation spectroscopy for determination of sex and species of mosquitoes in flight," *J. Biophotonics,* vol. 11, 2018.
38. A. P. Genoud, R. Basistyy, G. M. Williams, and B. P. Thomas, “Optical remote sensing for monitoring flying mosquitoes, gender

identification and discussion on species identification," *Applied Physics B,* vol. 124, p. 46, February 17 2018.

39. M. Sikulu, G. F. Killeen, L. E. Hugo, P. A. Ryan, K. M. Dowell, R. A. Wirtz, S. J. Moore, and F. E. Dowell, "Near-infrared spectroscopy as a complementary age grading and species identification tool for African malaria vectors," *Parasit. Vectors,* vol. 3, p. 49, 2010.
40. A. P. Hill, P. Prince, E. Piña Covarrubias, C. P. Doncaster, J. L. Snaddon, and A. Rogers, "AudioMoth: Evaluation of a smart open acoustic device for monitoring biodiversity and the environment," *Methods in Ecology and Evolution,* vol. 9, pp. 1199-1211, 2018.
41. P. Jancovic and M. Köküer, "Bird species recognition using unsupervised modeling of individual vocalization elements," *IEEE/ACM Transactions on Audio, Speech, and Language Processing,* vol. 27, pp. 932-947, 2019.

Fig. 1. **a)** Entomological-lidar system and its main components overlooking the *Jardin de los sueños* private forest, during a clear moment (17:30). **b)** Photo displaying the top of canopies at ~30 m over ground disappearing into the mist (9:30), **c)** A view from lidar toward valley at noon (12:05), typical of the field campaign days. The mist is impenetrable. **d)** Ecological studies in tropical virgin forests are challenging due to topography, tall vegetation structure, and stratification of ecological niches, here two chiroptologists install a bat net 20 m above ground.

Fig. 2. Lidar transect: **a)** Top view from an overcast satellite image of the cloud forest. The laser beam terminates in the valley after propagating almost 3 km. **b)** The field site is on the intermediate lowlands, and is part of the great pacific rainforest *El Chocó*, descending from the Andes to the Pacific Coast. **c)** The

beam was sent 4.5° inclined through the valley, at times with vegetation on both sides. **d)** Average vegetation height from space-borne lidar, the darker green areas indicate primary forest. **e)** Despite limited visibility by eye, an infrared near-infrared (0.8-1 μm) camera can at times form an image of the coffee plantation 3 km away where the beam terminates. The tall vegetation at closer range is seen on both sides of the beam. A nighttime image is superimposed in red to display the backscattering in the air and the beam remote termination spot.

Fig. 3. Technical details of the dual-band lidar system. **A)** Close-up of dual-band laser diode assembly. The emission cones of two multimode laser diodes with fast-axis-collimators (FACs) are combined by a dichroic shortpass beamsplitter on a precision alignment stage. **b)** Schematics of the Scheimpflug lidar system. The sensor strobe signal alternates the laser driver between dark, 808 nm and 980 nm. **c)** Spectral overview displaying the CMOS array sensitivity and the emission of the two lasers. The reflectance model for insect targets with three different equivalent pathlength of pure melanin is displayed for reference. **d)** Thin film model of the resonant backscatter for the two lidar bands as a function of typical insect wing thicknesses.

Fig. 4. Lidar data: **a)** The first half hour of the reported pilot field test is displayed in a time-range lidar map. Each column in the map represents a 6 s datafile. The maxima values of 980 nm backscatter are displayed as red, maxima of 808 nm are displayed as green and, median values of 808 nm, which

is insensitive to insects, are displayed as blue. The beginning represents a rare occasion with a signal visible all the way to the termination 3 km away, the visibility then decreases, and light is extinguished within the first 100 m. Insects show up as green dots on the map and bats display strong echoes in both bands. Fireflies were also observed both visually and by the instrument. These signals are unrelated to the modulation of the lasers and their actual distance cannot be deduced. **b)** Range resolved spectrogram of the lidar data illustrated by a 3D isosurface. The signal from the air and fog contributes low frequencies and is displayed in blue at the bottom of the plot. Two insects with distinct wing beat frequencies intercept the beam at a 100 m distance. The mean echo is displayed in the back panel in linear scale, the signal is dominated by an intense peak from a cloud layer at a 300 m distance, and smaller echoes from the two insects and the termination are also seen. Note that the contrast between fog and insects is poor in the echo intensity domain but great in the frequency domain.

Fig. 5. Example of insect observation by the dual-band lidar: **a)** Dual-band range-time displaying fast oscillatory insect observation *vs.* the slowly changing fog layer. **b)** Average echo of the same data; insect, fog, and termination features are seen at 90, 300, and 2929 m distance respectively. The 980 nm signal is generally one magnitude weaker, but the insect echo is relatively stronger for 980 nm due to the lower atmospheric scattering coefficient and lower absorption by melanin. **c)** Time series of the two bands composed of an oscillatory part from the wings and a bias envelope from the

body, the insert displays the reproducibility of the waveform. **d)** In the corresponding power spectrum, the fundamental tone is not necessarily the strongest, but in this case, the second overtone is.

Fig. 6. Lidar observation of a low frequent moth **a)** Dual-band time-range map; dense fog is seen as a gradient across the map. The apparent size was estimated to be 84 mm. The oscillatory extinction of the moth reduces the following backscatter from the fog and periodic shades are seen, e.g., at t_{moth}, when the wing has a maximal cross-section. **b)** Comparison of echoes from fog, t_{fog}, and from fog extinguished by the moth, t_{moth}. A small effect of the extinction is seen. The signal reaches noise levels after 200 m, for visual guidance two exponential decays are inserted with extreme atmospheric attenuation coefficients, μ_{att}, of 16 and 20 km^{-1}. **c)** Time series of the two bands composed of an oscillatory part from the wings and a stronger bias envelope from the body (as compared to Fig. 5c). **d)** In the corresponding power spectrum, the fundamental tone is the strongest.

Fig. 7. Dynamics of the backscattering signal from the moth in the two wavelength bands. The color of the arrows indicates time from 0 to 240 ms and the length indicates speed. The signals are not simply co-varying (i.e., they are not linearly correlated). On this slightly challenging graph, repeated features can be observed from the consecutive wingbeats. During each cycle, both left and right wings produce a peak and they show also higher melanin absorption

on the dorsal side for further differentiation of the signals. Melanization is higher on the dorsal side of the wings. The downstrokes appear straight and fast whereas the upstrokes appear wavy and slower.

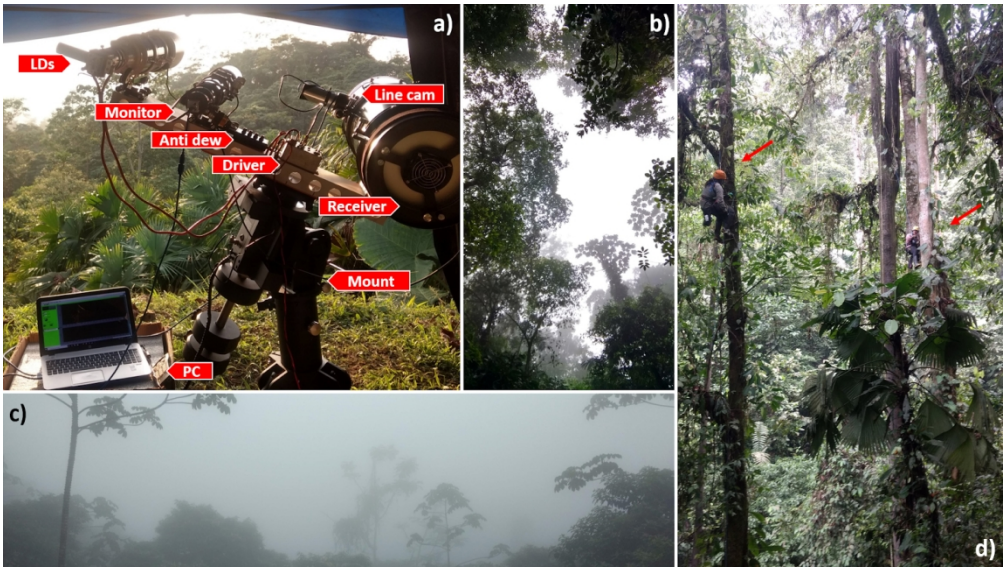

Fig. 1. a) Entomological-lidar system and its main components overlooking the Jardin de los sueños private forest, during a clear moment (17:30). b) Photo displaying the top of canopies at ~30 m over ground disappearing into the mist (9:30), c) A view from lidar toward valley at noon (12:05), typical of the field campaign days. The mist is impenetrable. d) Ecological studies in tropical virgin forests are challenging due to topography, tall vegetation structure, and stratification of ecological niches, here two chiroptologists install a bat net 20 m above ground.

135x76mm (300 x 300 DPI)

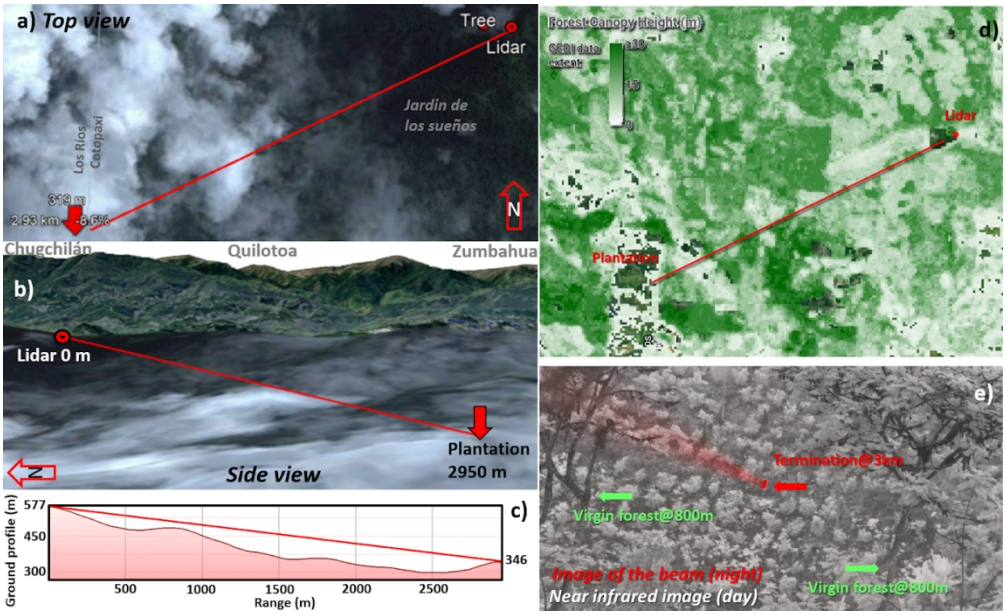

Fig. 2. Lidar transect: a) Top view from an overcast satellite image of the cloud forest. The laser beam terminates in the valley after propagating almost 3 km. b) The field site is on the intermediate lowlands, and is part of the great pacific rainforest El Chocó, descending from the Andes to the Pacific Coast. c) The beam was sent 4.5° inclined through the valley, at times with vegetation on both sides. d) Average vegetation height from space-borne lidar, the darker green areas indicate primary forest. e) Despite limited visibility by eye, an infrared near-infrared (0.8-1 μm) camera can at times form an image of the coffee plantation 3 km away where the beam terminates. The tall vegetation at closer range is seen on both sides of the beam. A nighttime image is superimposed in red to display the backscattering in the air and the beam remote termination spot.

116x70mm (300 x 300 DPI)

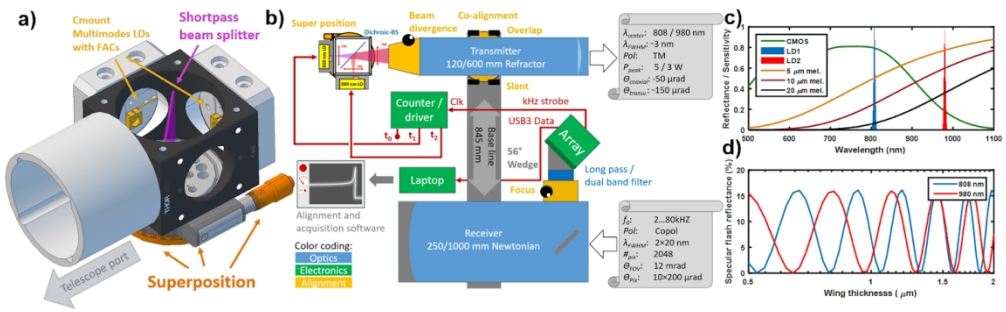

Fig. 3. Technical details of the dual-band lidar system. A) Close-up of dual-band laser diode assembly. The emission cones of two multimode laser diodes with fast-axis-collimators (FACs) are combined by a dichroic shortpass beamsplitter on a precision alignment stage. b) Schematics of the Scheimpflug lidar system. The sensor strobe signal alternates the laser driver between dark, 808 nm and 980 nm. c) Spectral overview displaying the CMOS array sensitivity and the emission of the two lasers. The reflectance model for insect targets with three different equivalent pathlength of pure melanin is displayed for reference. d) Thin film model of the resonant backscatter for the two lidar bands as a function of typical insect wing thicknesses.

135x42mm (300 x 300 DPI)

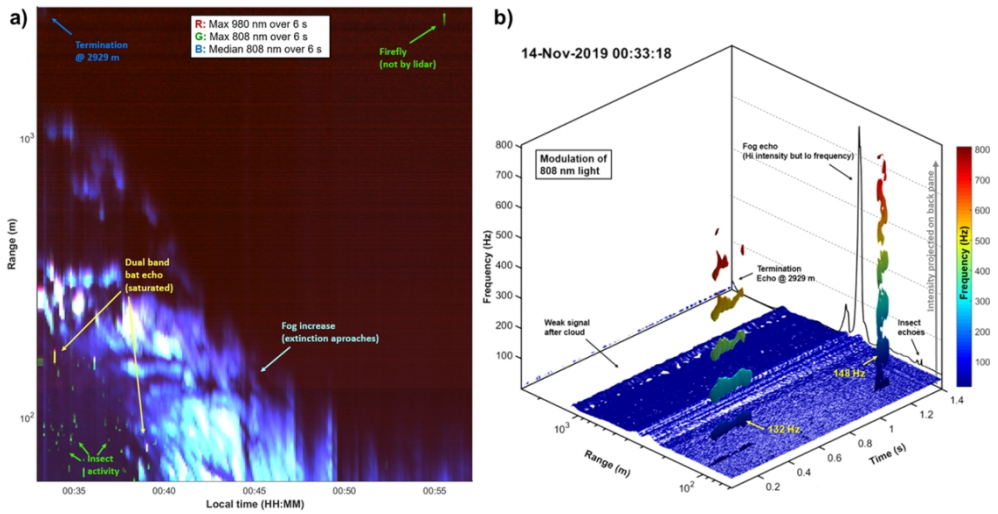

Fig. 4. Lidar data: a) The first half hour of the reported pilot field test is displayed in a time-range lidar map. Each column in the map represents a 6 s datafile. The maxima values of 980 nm backscatter are displayed as red, maxima of 808 nm are displayed as green and, median values of 808 nm, which is insensitive to insects, are displayed as blue. The beginning represents a rare occasion with a signal visible all the way to the termination 3 km away, the visibility then decreases, and light is extinguished within the first 100 m. Insects show up as green dots on the map and bats display strong echoes in both bands. Fireflies were also observed both visually and by the instrument. These signals are unrelated to the modulation of the lasers and their actual distance cannot be deduced. b) Range resolved spectrogram of the lidar data illustrated by a 3D isosurface. The signal from the air and fog contributes low frequencies and is displayed in blue at the bottom of the plot. Two insects with distinct wing beat frequencies intercept the beam at a 100 m distance. The mean echo is displayed in the back panel in linear scale, the signal is dominated by an intense peak from a cloud layer at a 300 m distance, and smaller echoes from the two insects and the termination are also seen. Note that the contrast between fog and insects is poor in the echo intensity domain but great in the frequency domain.

108x59mm (300 x 300 DPI)

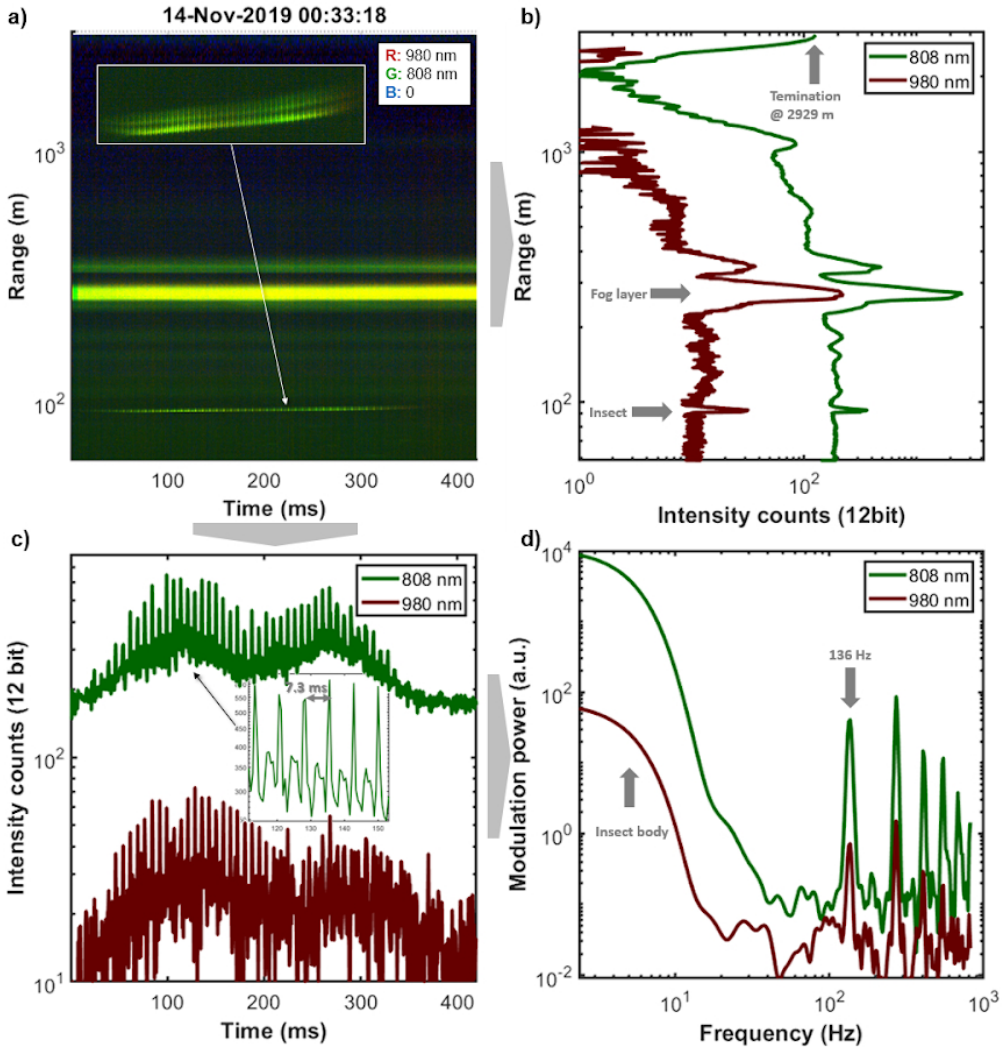

Fig. 5. Example of insect observation by the dual-band lidar: a) Dual-band range-time displaying fast oscillatory insect observation vs. the slowly changing fog layer. b) Average echo of the same data; insect, fog, and termination features are seen at 90, 300, and 2929 m distance respectively. The 980 nm signal is generally one magnitude weaker, but the insect echo is relatively stronger for 980 nm due to the lower atmospheric scattering coefficient and lower absorption by melanin. c) Time series of the two bands composed of an oscillatory part from the wings and a bias envelope from the body, the insert displays the reproducibility of the waveform. d) In the corresponding power spectrum, the fundamental tone is not necessarily the strongest, but in this case, the second overtone is.

72x76mm (300 x 300 DPI)

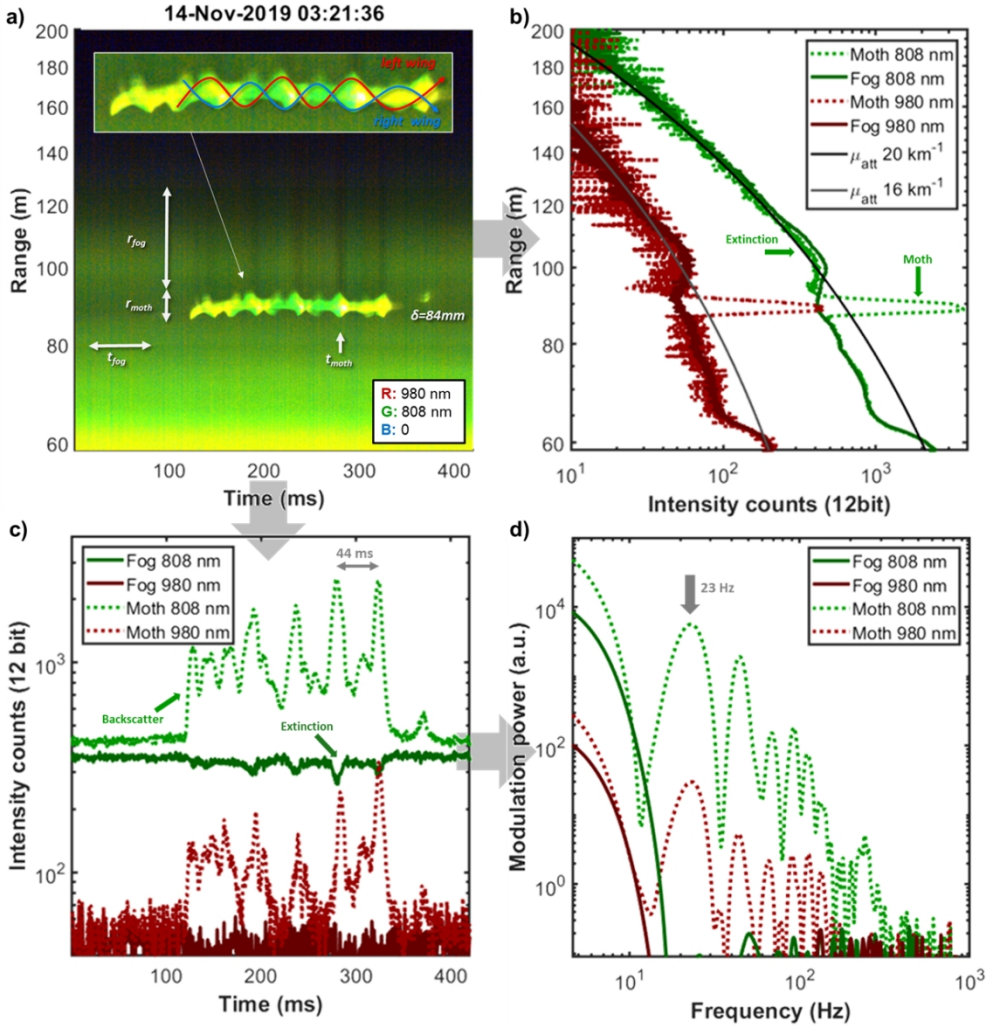

Fig. 6. Lidar observation of a low frequent moth a) Dual-band time-range map; dense fog is seen as a gradient across the map. The apparent size was estimated to be 84 mm. The oscillatory extinction of the moth reduces the following backscatter from the fog and periodic shades are seen, e.g., at tmoth, when the wing has a maximal cross-section. b) Comparison of echoes from fog, tfog, and from fog extinguished by the moth, tmoth. A small effect of the extinction is seen. The signal reaches noise levels after 200 m, for visual guidance two exponential decays are inserted with extreme atmospheric attenuation coefficients, μatt, of 16 and 20 km-1. c) Time series of the two bands composed of an oscillatory part from the wings and a stronger bias envelope from the body (as compared to Fig. 5c). d) In the corresponding power spectrum, the fundamental tone is the strongest.

104x108mm (300 x 300 DPI)

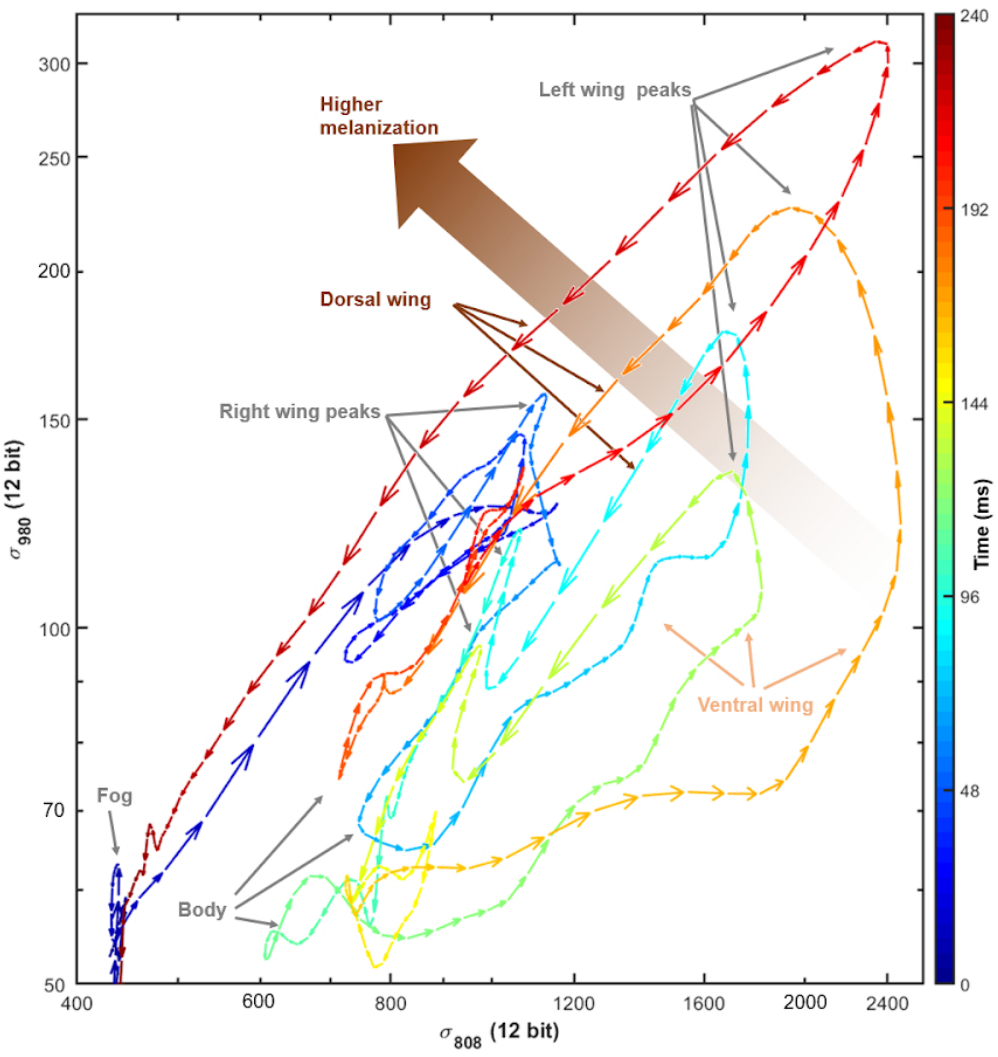

Fig. 7. Dynamics of the backscattering signal from the moth in Fig.6c. Each arrowhead indicates raw unfiltered backscatter intensity counts for consecutive time samples for the 808 and 980 nm bands. The color of the arrows indicates time from 0 to 240 ms and the length indicates speed. The signals are not simply co-varying (i.e., they are not linearly correlated). On this slightly challenging graph, repeated features can be observed from the consecutive wingbeats. During each cycle, both left and right wings produce a peak and they show also higher melanin absorption on the dorsal side for further differentiation of the signals. Melanization is higher on the dorsal side of the wings. The downstrokes appear straight and fast whereas the upstrokes appear wavy and slower.

72x76mm (300 x 300 DPI)

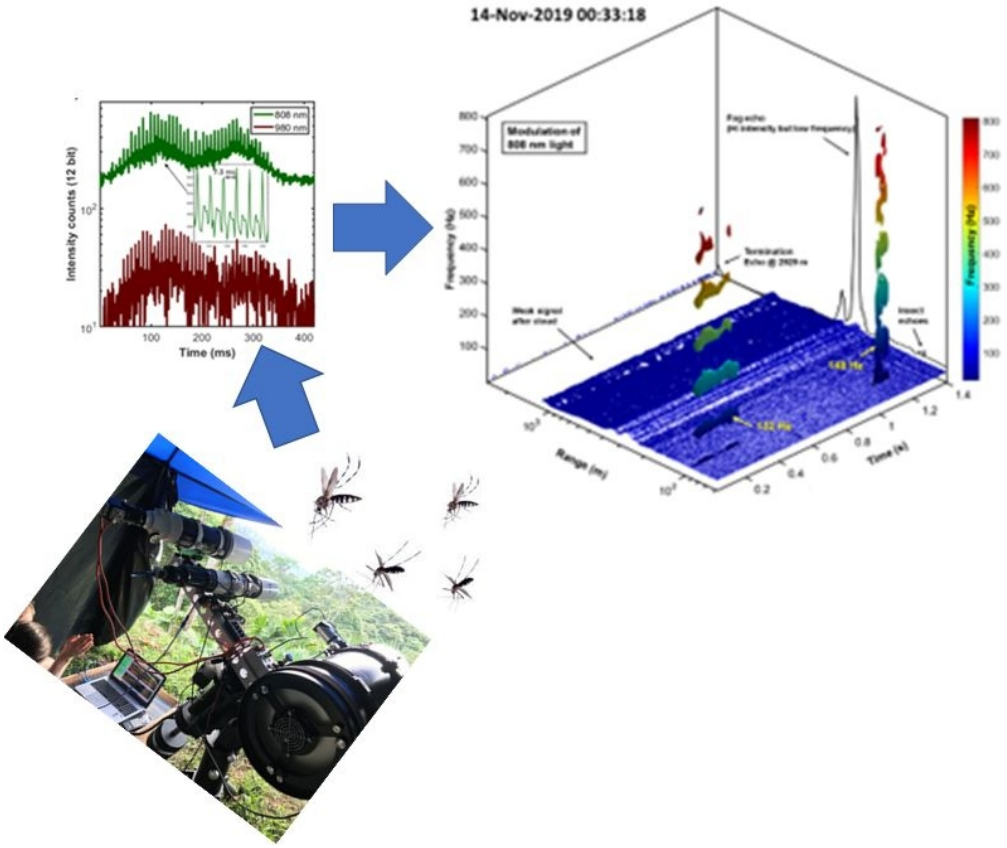

280x245mm (72 x 72 DPI)